Conductometric and electrooptic key quantities characterizing electric pore formation in cellular and lipid model membranes

Dissertation zur Erlangung des
Doktorgrades der Naturwissenschaften
an der Universität Bielefeld

von

Catalin Gabriel Frantescu
Bielefeld, September 2007

for my family,

Alina

Maria

Elena

Contents:

Part I. Single cell electroporation. -Abstracts

1. **C. G. Frantescu, U. Pliquett, E. Neumann**, Electroporation of single CHO cells, 11. Heiligenst. Koll. (Dieter Beckmann, Manfred Meister, Eds.), 2002, pp. 543-549.

A lipid membrane, artificial or natural, can become permeable by exposure to a brief high-intensity electric field pulse, causing membrane electroporation. In the electroporated state a lipid membrane is highly permeable to small ions and even macromolecules.

Electroporation is a commonly employed method for gene transfer and for the transport of other normally impermeant molecules into cells. Electroporation is a candidate method for enhancing drug delivery across the skin into organs. Further optimizations of application protocols require advanced investigations on the membrane level.

Besides the desired electrically mediated transport, electroporation exhibits some side effects. For instance, JOULE heating can diminish cell survival or even lead to irreversible damage.

The aim of this study is to characterize the electroporation process in term of different pore states.

2. **U. Pliquett, C. G. Frantescu, E. Neumann**, Unsymmetrische Elektroporation bei Depolarization und Hyperpolarization von CHO-Zellmembranen, 11. Heiligenst. Koll. (Dieter Beckmann, Manfred Meister, Eds.), 2002, pp. 135-142.

Die Transmembranspannung von Zellen im Gewebeverband ist einer Messung über makroskopische äußere Elektroden nicht zugänglich, da sich die Spannungen über die jeweils gegenüberliegenden Seiten der Zellmembran aufheben. Durch eine einseitige temporäre Permeabilisierung der Zellmembran summieren sich die Beiträge der entgegengesetzten Seite, wodurch an den Elektroden eine von der Struktur der Membran sowie der ionischen Kanäle und Pumpen abhängige Spannung gemessen werden kann. Es wird gefunden, daß die Membranelektroporation stark unsymmetrisch ist. Bei depolarisierenden Pulsen tritt die Elektropermeabilisierung im Bereich U_M = 0.5±0.1 V auf, während bei hyperpolarisierenden Pulsen der Bereich U_M = -0.95±0.15 V ist.

3. **C. G. Frantescu, U. Pliquett, E. Neumann**, The membrane impedance before and after electroporation of single Chinese Hamster Ovary cells, 12. Heiligenst. Koll. (Dieter Beckmann, Manfred Meister, Eds.), 2004, pp. 217-224.

When exposed to electric field pulses, lipid bilayer membranes become permeable to ionic molecules and macromolecules, which usually can not pass the dielectric part of the membrane. This electric field effect is called membrane (MEP) electroporation. Nowadays, this field method is used for cell transfection with naked DNA [1]. Another powerful application of MEP is the enhancement of drug delivery especially for charged species [2; 3]. Although the mechanism of MEP is slowly being understood, the optimization of electrical protocols still faces the problem of the only partially known interactions of the external field pulse with the cell membranes.

Here, the electric resistance and capacitance of intact single cells are measured before and after electroporation. Since the field-induced structural changes in the membranes persist a long time after short-pulse electroporation (milliseconds up to seconds), conventional impedance techniques in the frequency domain are not applicable. Therefore, we use a time domain approach monitoring the voltage change caused by rectangular current wave excitation.

The experiments are performed in the whole cell clamp configuration of selected single cells [4]. The advantages of this technique as compared to measurements in tissue or cell suspension are: (i) the access to a single membrane, (ii) the equally weighting of the entire membrane, no angle dependence and no averaging over membranes with arbitrary orientations, (iii) the application of depolarizing or hyperpolarizing pulses, with respect to the natural membrane potential, here $\Delta\varphi_{nat} = -60 \pm 30mV$.

In the case of single cells, Joule heating is shown to be negligibly small.

4. **U. Pliquett, H. Krassen, C. G.Frantescu, D. Wesner, E. Neumann, K. Schoenbach**, Asymmetric changes in membrane conductance due to hyper- and depolarization: probing with current and voltage clamp, IFMBE Proc., 2005, pp. 1924-1229.

Cell membranes are composed differently at the cytosolic and the extracellular side. This has a strong effect on the current-voltage characteristics (CVC) even if voltage gated channels are ignored. While a decrease of the conductance for small superimposed transmembrane voltages (<0.5 V) was found when chinese hamster ovary cells (CHO)–cells with no excitable plasma membrane hyperpolarized, the conductance rose as soon as a depolarizing voltage was applied. At higher voltage, both hyper- and depolarized membranes showed electroporation, but at different thresholds. Probing the CVC with controlled current or controlled voltage yields quite different results because of the variable voltage divider between the membrane and the electrolytes, which yields a positive feedback for voltage clamp condition but a negative feedback under current clamp condition. This also influences the results of pulsed field experiments in low (negative feedback) and highly conductive (positive feedback) media, indicating, for instance, a lower electroporation threshold of cells in tissues.

Part II. Solid-state supported bilayers

1. Concepts and theory

The cellular membrane is a lipid bilayer system with embedded proteins. These proteins have a variety of functions, e.g. transport of membrane impermeable molecules or anchoring the membrane to the cytoskeleton. This complexity makes investigations of the interaction between lipid molecules and electric field very difficult. To simplify the system, the solid supported bilayer model has been proposed. This model has several advantages but also drawbacks. The first, and major, advantage is that the composition of this bilayer is chemically controlled. Using different techniques, the desired lipids can be deposited on to the bottom or top monolayer. This has repercussions on the behavior of the bilayer as a system. The main drawback is that the surface of this planar bilayer is very sensible and breaks easily. This yielded also the difficulty with the experimental part.

In the presence of an electric field, the lipid molecules rearrange themselves due to the interactions of the lipid dipole moment with the electric field. Additionally, thermal motion and local defects, force the creation of aqueous pathway across the lipid portion of the membrane. This structural change on membrane level, induced by an outer electric field is called electroporation.

This effect has a tremendous impact on living cells, tissues and even organs. Due to the concentration gradient, charged molecules and even macromolecules can be exchanged between the extra- and intracellular medium.

An emerging application of electrically enhanced membrane transport is gene transfer which consist in transporting "naked" DNA (linear shaped double stranded DNA fragments) to the cytoplasmic side of the cell [1; 2]. This causes the cell to express proteins, usually not coded by the cells wild type DNA. Another application is electro-chemotherapy, where the aim is to reduce the side effects of chemotherapy simultaneous with increasing the efficacy of the treatment. The method consists in the application of a short high voltage pulse across the tumor region after the injection of the drug. The uptake of the drug is increased, in some cases by several orders of magnitude [3; 4]. Therefore, the net application of the drug can be reduced.

These important applications need a deeper understanding of the phenomena involved and ask for further investigations in this field. The objective has been the study of the

orientation of lipid molecules in the presence of an electric field using electrical and optical methods.

2. Electro-thermodynamics of membrane electroporation

Membrane electroporation can be modelled as a cooperative transition of a number *m*, (*m* ≈12) of lipid molecules from a closed membrane state (*C*) to a porous state (*P*) [5].

$$(C) \underset{-k_p}{\overset{k_p}{\rightleftharpoons}} (P) \qquad (1)$$

In the overall-scheme (1), k_p represents the overall poration rate coefficient and k_{-p} is the overall resealing rate coefficient.

The pore formation involves water entrance into the membrane.

The degree of membrane electroporation is given by:

$$f_p = \frac{[P]}{[P]+[C]} = \frac{K}{1+K} \qquad (2)$$

For the overall-scheme (1), the equilibrium constant, is defined as:

$$K = \frac{[P]}{[C]} = \frac{f_p}{1-f_p} = \frac{k_p}{k_{-p}} = \exp[-\Delta_r \hat{G}^{\ominus} / RT] \qquad (3)$$

where *K* is related to the transformed Gibbs reaction energy: $\Delta_r \hat{G}^{\ominus}$. Starting from the non-equilibrium condition:

$$\Delta_r \hat{G} = \Delta_r \hat{G}^{\ominus} + RT \ln Q \qquad (4)$$

where $\Delta_r \hat{G}^{\ominus} = \hat{G}_m^P - \hat{G}_m^C$ is the standard (for 1molar transition) value of the electrochemical Gibbs reaction energy, $R = k_B \cdot N_A$ is the gas constant (R = 8,31 J · K^{-1} · mol^{-1}), k_B the Boltzmann constant (k_B = 1,38 × 10^{-23} J· K^{-1}), N_A the Loschmidt-Avogadro constant (N_A = 6,022 ×10^{23} mol^{-1}), T the absolute (Kelvin) temperature.

In Eq.(4), where $\Delta_r \hat{G} = \sum \nu_j \hat{\mu}_j$, the quantity $\hat{\mu}_j = \mu_j - \int M_j dE$ is the dipolochemical potential for a component j present in its activity $a_j = c_j y_j / c^{\ominus}$, where, respectively, c_j is the concentration and y_j, the thermodynamic activity coefficient of the component or state j and $c^{\ominus} = 1M$ is the concentration unit. The term $M_j = N_A \langle m_j \rangle$ is the molar

moment, $\langle m_j \rangle$ the mean molecular moment of j, and E = U/l the field strength, where U is the voltage and l the distance of the electrical potential drop Δφ = -U.

The nonequilibrium ratio of activities is given by $Q = \prod_j a_j^{\nu_j}$; the stochiometric numbers ν_j count positive for products and count negative for educts.
At equilibrium, in the presence of E,

$$\Delta_r \hat{G} = 0 \text{ and } \qquad Q_{eq} = K \qquad (5)$$

Insertion into Eq. (4), yields:

$$RT \ln K = -\Delta_r \hat{G}^{\ominus} \qquad (6)$$

and this in to Eq. (3) results in:

$$K = \exp[-\Delta_r \hat{G}^{\ominus} / RT] \qquad (7)$$

Insertion of Eq. (7) into Eq. (2) yields the overall electroporation degree:

$$f_p = \frac{e^{-\Delta_r \hat{G}^{\theta}/RT}}{1 + e^{-\Delta_r \hat{G}^{\theta}/RT}} \ , \qquad (8)$$

thus connecting the experimental quantity f_p with the electrothermodynamic quantity $\Delta_r \hat{G}^{\ominus}$.

For those common cases of analysis where $f_p << 1$, usually $f_p \leq 10^{-2}$, the approximation

$$f_p = K = e^{-\Delta_r \hat{G}^{\ominus}/RT} \qquad (9)$$

it practically justified.

The general (not yet E – transformed) Gibbs energy is given by the differential:

$$\mathrm{d}G = \sum_j \mu_j \mathrm{d}n_j + E\mathrm{d}M \qquad (10)$$

where μ_j are the ordinary chemical potentials, $\mu_j = \mu_j^{\theta} + RT \ln a_j$ the chemical potential of species *j* and $\mu_j^{\ominus}$ the standard chemical potential.

In the presence of an external electrical field ***E***, and with the macroscopic moment:

$$M = \sum M_j = N_A \sum_j \langle m_j \rangle \qquad (11)$$

the differential form of the transformed Gibbs energy is given by:

$$d\hat{G} = d(G - EM) \qquad (12)$$

Insertion of: $\mathrm{d}G = \sum_j \mu_j \mathrm{d}n_j + E\mathrm{d}M$ into Eq. (12), yields $\mathrm{d}\hat{G} = \sum_j \mu_j \mathrm{d}n_j - M\mathrm{d}E \leq 0$

where < refers to spontaneous reaction flow and = refers to the equilibrium state.

Applying the van't Hoff relation to field effects at constant p, T, we have:

$$\left(\frac{\partial \ln K}{\partial E}\right)_{p,T} = \frac{\Delta_r M}{RT} = \frac{\langle \Delta_r m \rangle}{k_B T} \qquad (13)$$

where the reaction dipole moment is defined as $\Delta_r M = (\partial M / \partial \xi) = \sum \nu_j M_j$.

Since $\hat{G} = G - EM$, *K(E)* can now be expressed as

$$K = K_0 \cdot e^{X(E)} \qquad (14)$$

where K_0 refers to K(E=0) at zero field.

The field factor is defined by: $X(E) = \frac{\int \Delta_r M dE}{RT}$ (15)

For membrane processes like $(C) \rightleftharpoons (P)$, the field factor is given by:

$$X_m = \frac{\int \Delta_r M dE_m}{RT} \qquad (16)$$

where E_m is the amplified membrane field.

If local membrane pore polarisation is considered ($\Delta M = \Delta P \cdot V$),

$$X_m = \frac{V \varepsilon_0 (\varepsilon_W - \varepsilon_L)}{2 k_B T} E_m^2 \qquad (17)$$

where $\Delta P = \varepsilon_0 (\varepsilon_W - \varepsilon_L) E_m$ and V is the average volume of one average pore.

In Eq.(17), ε_0 = 8,85419 x 10^{-12} Fm^{-1} is the vacuum permittivity;

ε_W = 80,1 – water dielectric constant at 20°C;

ε_L = 2,1 – lipid dielectric constant.

Since $K_m = K_m^0 \cdot e^{X_m(E_m)}$ contains V in the field factor $X_m(E_m)$, it is seen that the analysis of the data correlation (f(E),E) in terms of f as a function of E_m directly yields the polarisation volume of an average pore.

Applying, e.g., a cylindrical pore model, $V = d_m \cdot \pi \cdot \overline{r}_p^2$, with d_m = 5 nm, an average pore radius $\overline{r}_p = \sqrt{\overline{r_p^2}}$ is derived from data.

The membrane field strength E_m for single spherical cells in external fields E is dependent on the angular position θ, according to:

$$E_m(\theta) = \frac{3}{2} \cdot \frac{\overline{a}}{d_m} \cdot f_\lambda \cdot E \cdot |\cos\theta| \qquad (18)$$

where the experimental E_m is the θ – average given by:

$$E_m = \frac{\sqrt{3}}{2} \cdot \frac{\overline{a}}{d_m} \cdot f_\lambda \cdot E \qquad (19)$$

In Eqs. (18) and (19), $\overline{a}$ is the mean cell radius, $d_m \approx 5$ nm the dielectric thickness of the membrane and $f_\lambda \leq 1$ is the (so-called) conductivity factor [6].

For cells under patch clamp conditions, $E_m = U \cdot d_m$, where *U* is the applied voltage, is a very good approximation.

3. Lipid reorientation in membrane electroporation

It is recalled that electroporation is the creation of transient pathways or pores at the membrane level using electric fields. The degree of electroporation can be derived from the electric currents across the membrane at a given transmembrane voltage $U = U_m = E_m \cdot d_m = -\Delta\varphi_m$. In this case, only the conductive states of the pores can be obtained.

A defined proposal for the reorientation of the lipids, by organization in the electric membrane field, has been given already in 1982 [7]. The early theories about lipid reorientation proposed that first a hydrophobic pore (HO) is formed, and then, in the second step this pore transforms into a hydrophilic pore (HI). The proposal of 1982, however, does not consider the thermodynamically very unlikely HO-pore, but only the HI configuration.

The lipids of a membrane represent a fluctuating layer where the lipids rotate along their longitudinal axis and vibrate. A few water molecules can go into the hydrophobic part of the membrane for a short time only. If an electric field is applied across the lipid membrane, the lipid heads start to rearrange in the direction of the electric field and more and more water molecules insert themselves in the membrane until, finally, a hydrophilic pore is formed (Fig. 1).

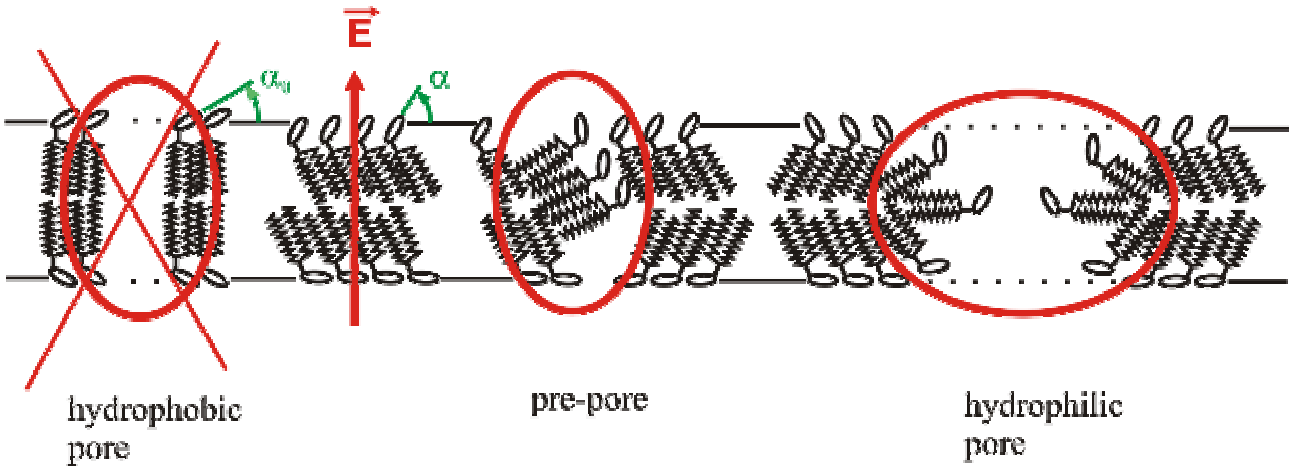

Fig. 1. Scheme for the lipid reorientations in an external electric field E, increasing the angle from α_0 to $\alpha(E)$. The water entrance increases the overall dielectric constant of the bilayer. Finally a hydrophilic pore is created.
Scheme by S. Kakorin, E. Neumann, D. Boeckmann, K. Grübmüller (2004)

4. Electrooptics and conductometry

One of the aims of this study has been to quantify the degree of electroporation in terms of the reorientation of the lipids in the bilayer. Electrically, the task has been to measure the impedance of the membrane, directly associated with the fractional area involved in electroporation.

The optical measurements have been aiming at the features of lipid orientation during electroporation. Due to the fact that the lipids have a negligible absorbance in the visible range of the electromagnetic spectrum, an indirect approach has been used. The lipid bilayer is marked with lipid-like chromophores which have a strong absorbance anisotropy and a precise average orientation in the membrane.

4.1. Surface plasmon resonance on solid bilayers

Refraction can be observed, when light passes an interface between different refractive index. If it approaches the interface from the optically denser medium under a flat angle, total reflection may occur. In this case all light energy is reflected from the surface. Closer examination of the phenomena yields an exponential decay of the light energy

behind the totally reflecting surface owing to the tunneling effect. If an absorbing structure is placed in this region, a part of the light energy is absorbed and thereby the energy of the reflected light decays.

When a metallic surface with the right crystal structure (i.e. gold, aluminum), is placed behind a totally reflecting surface, light can excite plasmons. Plasmons are density oscillations of freely movable electrons, i.e. in metals. If the metal layer is reasonably thin (50 nm), surface plasmons are excited, yielding a high electric field component above the metal. For a given wavelength of the incident light, the density of the plasmons depends on angle of incidence, thickness of metallic layer, index of refraction of the glass and type of metal [8].

Since part of the incident light is absorbed to create the plasmons, in the resonance case, the entire light energy is used to excite the plasmons. Therefore at the side of the detector the energy level is zero. The energy density of the plasmons decay exponentially and practically, after a few nm distance from the metal surface, the energy level is zero. Only objects within this range can interact with the electric field component arising from surface plasmons. This finally can be detected by a decreased energy of the reflected beam.

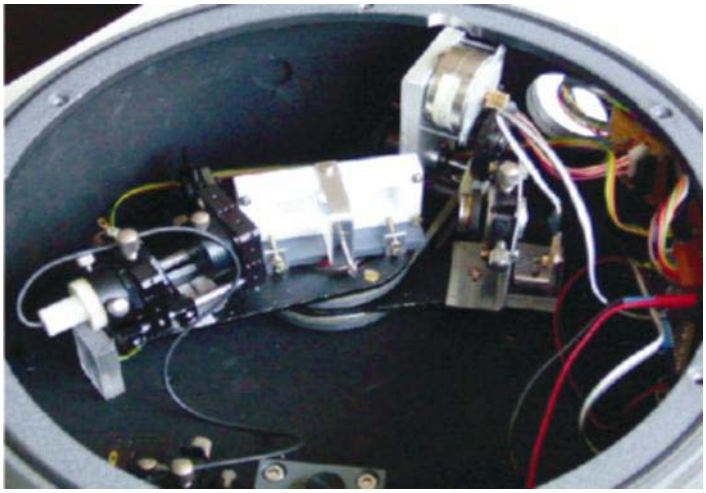

Fig. 2. Experimental SPR spectrometer.

The plasmon resonance effect has been used to detect the changes in the energy absorption when anisotropic lipid-like molecules, change orientation relative to the membrane normal. The experimental set-up used to detect the lipids movement is presented in Fig. 2.

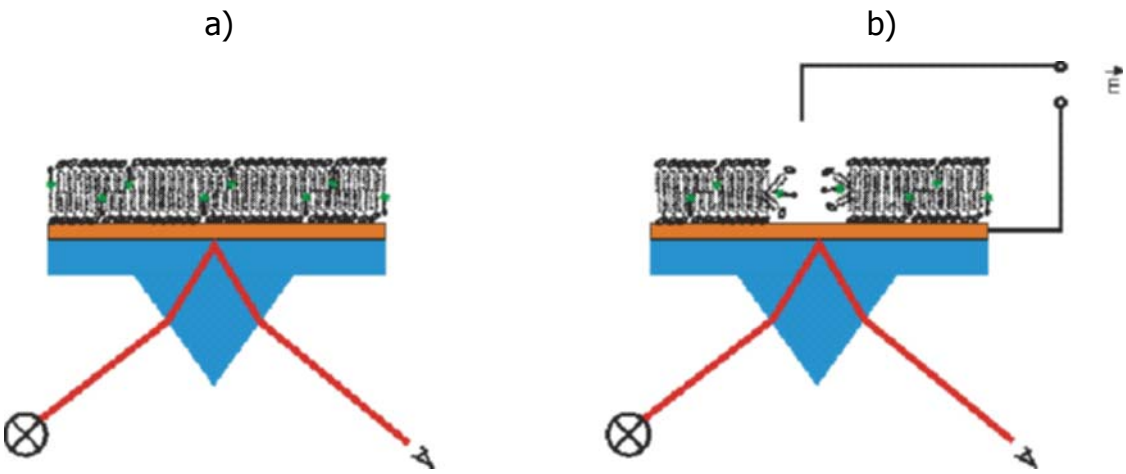

Fig. 3. Principle of a surface plasmon resonance measurement device.

In Fig. 3 are schematic represented the measurement principles of the surface plasmon resonance without the presence of the electric field (a) and in the presence of the electric field (b).

The problems encountered are: (1) the plasmons are excited at long wavelengths, e.g. at (λ > 600 nm); (2) Commercially available dyes absorb light at λ < 600 nm. Matlab© simulations of the Maxwell theory proved, indeed, that the plasmons are created in the red light range (λ > 630 nm).

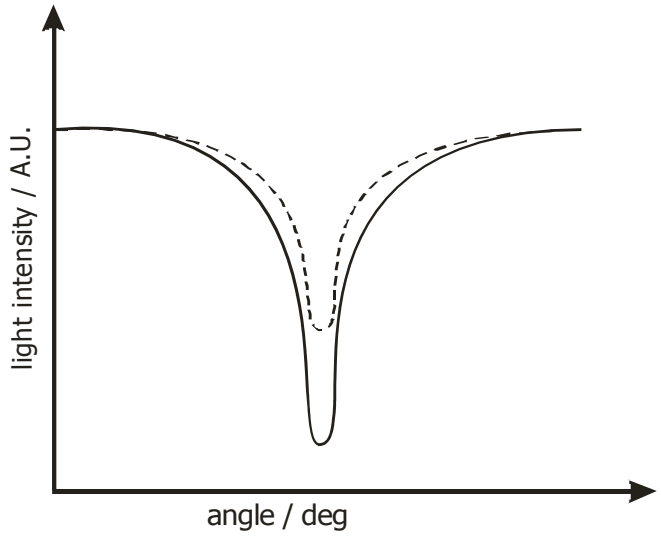

Fig. 4. Solid line – signal without electric field; dashed line – expected signal in the presence of membrane electroporation (MEP).

4.2. Ellipsometry

The second method used to investigate the orientation of lipids in the presence of the electric field is the ellipsometry. This method is based on the property of some materials to change the orientation of the electrical vector of the light (light polarization) [9; 10] by dipolar interaction. In a lipid bilayer doped with lipid-like dyes the intensity of the reflected light varies with the absorption of the bilayer, which is depends on the orientation of the dye. For this type of investigation the aim has been to determine the changes ratio between sagittal and parallel polarization. For this the experimental ellipsometer (Fig. 5) has been constructed.

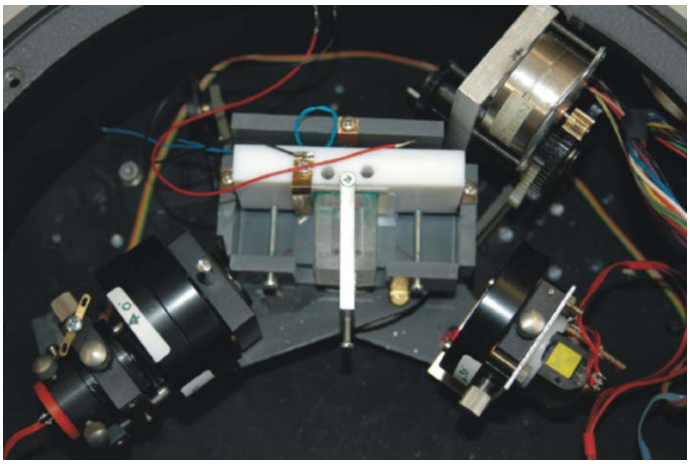

Fig. 5. Picture of the experimental ellipsometer.

The light, unpolarized initially, or with an arbitrary polarization, is transformed into circular polarized light by means of a $\lambda/4$ plate (Fig. 6) then, the light it is reflected by the sample and the parallel and sagittal component is detected using an polarizing beam splitter with attached detectors. The apparatus was mounted on a goniometric head in order to adjust the angle of incidence (Fig. 5).

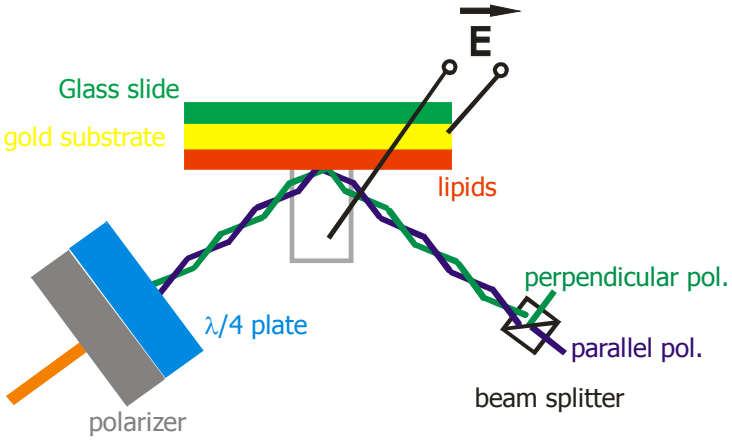

Fig. 6. Schematic of the ellipsometer.

When the dipole moment of the optical probes is parallel with the polarization of the light then the energy transfer approaches a maximum. This yields a maximum in the absorption of the optical probes as well. In the Fig. 7 are presents the theoretical answers of the ellipsometrical approach.

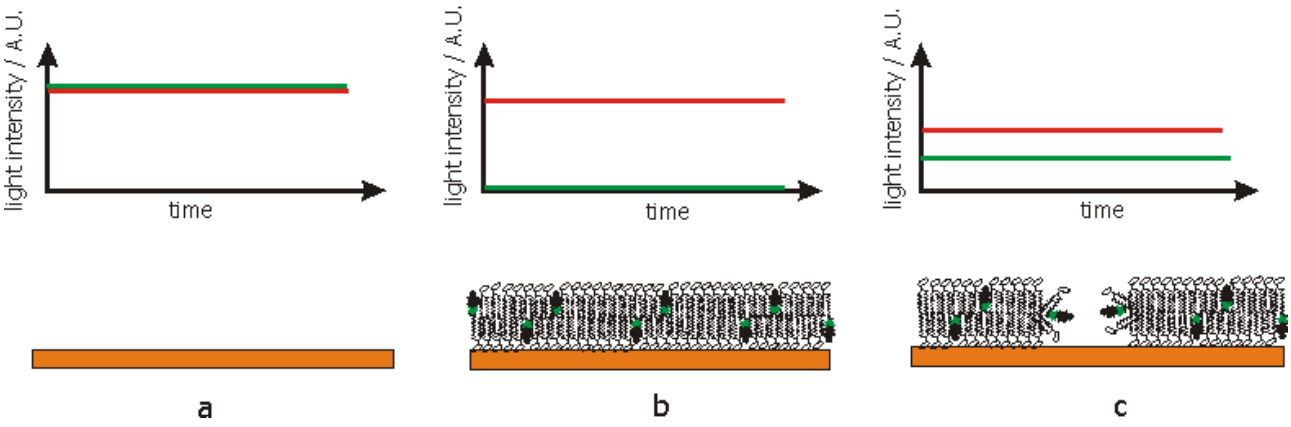

Fig. 7. Ellipsometric measurement

a) the clean gold surface used as a support for the bilayer reflects with the same intensity both light polarizations (red – parallel with the surface; green – sagittaly to the surface);

b) the optical probes form the bilayer absorbs the sagittal component of the light when they are orientated perpendicularly to the surface;

c) the optical probes reorientation together with lipids modify the absorption ratio between perpendicular and parallel light polarization;

With the system initially calibrated, that both polarizations have the same intensity in the case of bare gold surface it is possible to monitor the orientation of the optical probes within the bilayers (Fig.7). The main advantage of this method is a much greater

wavelength tolerance, but paying attention at the gold reflectivity at the desired wavelength.

4.3. Materials and methods

4.3.1. Construction of devices

The Surface Plasmon Resonance (SPR) spectrometer implies the existence of a light source, a sample to be analyzed and a detector (Fig. 8). The angles between the light source and the normal to the sample surface and between the detector and the normal to the surface, should be equally and variable. This implies different mechanical solutions such as: (i) fixed light sources, movable sample and movable detector (with a double angular speed than the sample), method used in the case of big light sources like gas lasers or (ii) fixed sample and movable light source and detector (each with the same angular speed but different directions) like in the present case. The advantages of this approach are: (i) simple mechanical construction, (ii) auto synchronization for the angles based on a single electric motor.

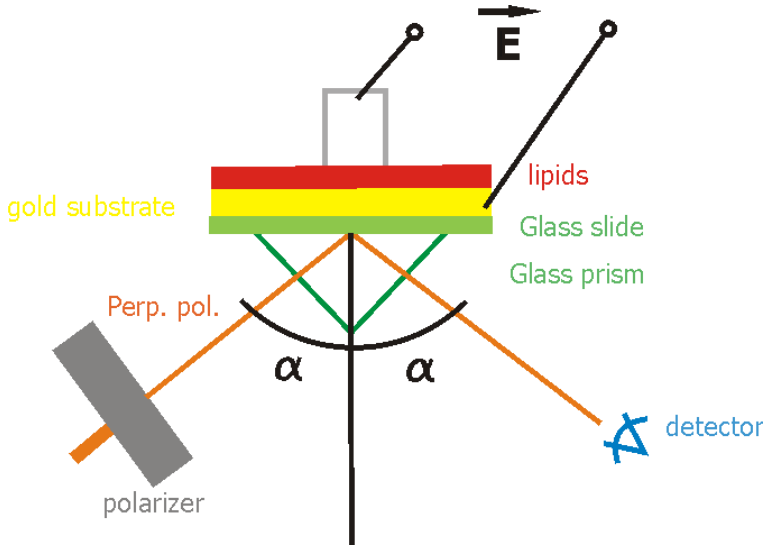

Fig. 8. SPR spectrometer.

The light source is an exchangeable module. A laser light source has been chosen because of the high intensity, high stability and small beam divergence. The small divergence of the beam eliminates the need of collimating lenses.

The main problem of SPR is that for plasmons excitation, long wavelengths are needed (λ

≥ 600 nm). For the gold layer in this study, a red laser diode (λ = 650 nm) was selected.

The theoretical investigations of plasmons generation are based on Frensel's equations [11] for a prism – metal – medium system (Fig. 9).

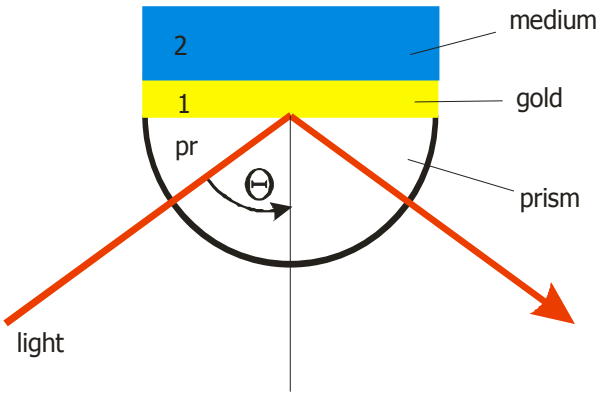

Fig. 9. Schematic diagram of Atenuated Total Reflected (ATR) coupler.

For the three layers system the total reflectance is:

$$R = \left| \frac{r_{pr1}^{p} + r_{12}^{p} \cdot e^{2 \cdot i \cdot k_{z1} \cdot d_1}}{1 + r_{pr1}^{p} \cdot r_{12}^{p} \cdot e^{2 \cdot i \cdot k_{z1} \cdot d_1}} \right|^2 \quad \text{where:} \qquad (20)$$

r_{pr1}^{p} is the reflectance contribution between prism and gold;

r_{12}^{p} is the reflectance contribution between gold and medium;

$k_{z1} \cdot d_1$ is the optical path length in the thickness of the gold layer.

The best optical probe for this kind of experiments should have the following characteristics: (i) - similar dimensions as lipid molecules in order to maintain the geometry of bilayer; (ii) – the active part of the probe should be anisotropically for detection of its orientation.

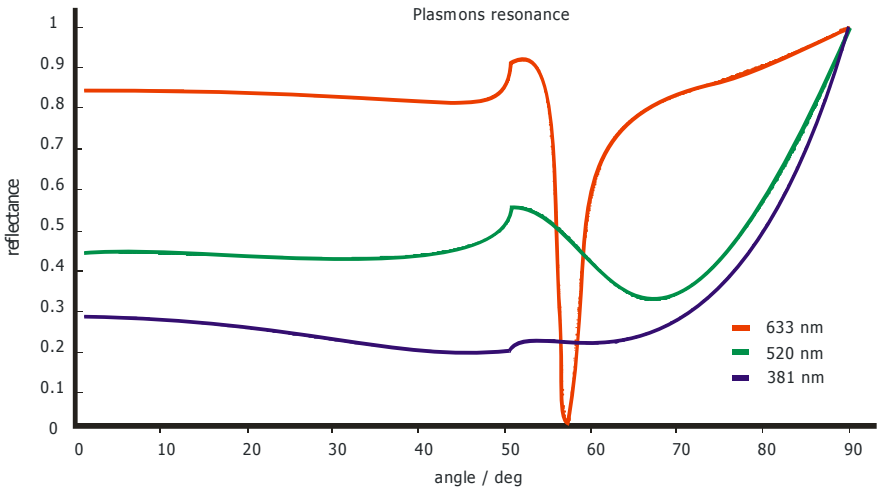

Fig. 10. Plasmons resonance for different wavelengths using an SF10 glass prism (n = 1,723), 50 nm gold thickness and water (n = 1,333) as medium.

Using the Frensel's equations [11], the resonance effects where simulated (Fig. 10), to determine the minimum usable wavelength for the experiments.

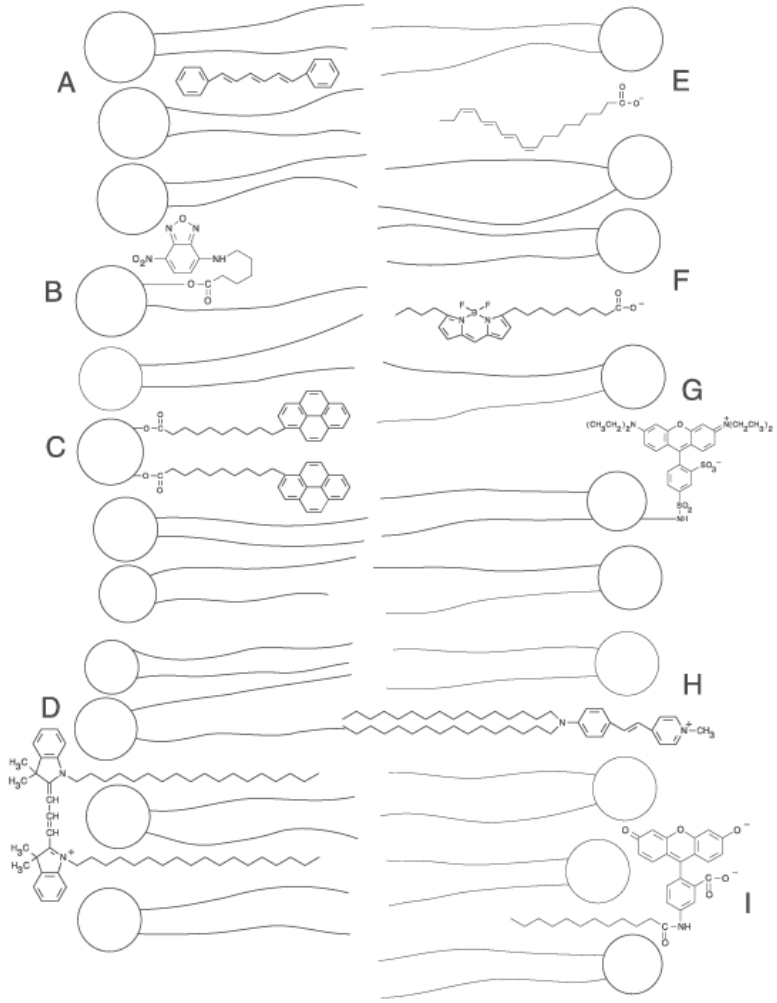

Fig. 11. Commercially available dyes for lipid membranes (Molecular Probes - Invitrogen Corporation, California, USA).

Location and orientation of representative fluorescent membrane probes in a phospholipid bilayer: **A)** DPH (D202), **B)** NBD-C_6-HPC (N3786), **C)** bis-pyrene-PC (B3782), **D)** DiI (D282), **E)** *cis*-parinaric acid (P36005), **F)** BODIPY 500/510 C_4, C_9 (B3824), **G)** *N*-Rh-PE (L1392), **H)** DiA (D3883) and **I)** C_{12}-fluorescein (D109).

The commercially available optical probes are presented in Fig. 11. The best candidates, from the chromophore orientation point of view, are type A, F and H, but the absorbance for these types are: 350 nm for type A, 581 nm for type F and 491 nm for type H.
The lack of proper optical probes stopped further experiments because all the commercially available optical probes absorb at wavelengths lower than 650 nm.

The next technique used for experiments has been the ellipsometry. The ellipsometry is based on the interaction between polarized light and samples. Based on the sample orientation a different amount of the incident energy can be absorbed by the sample and detected afterwards as a smaller intensity.

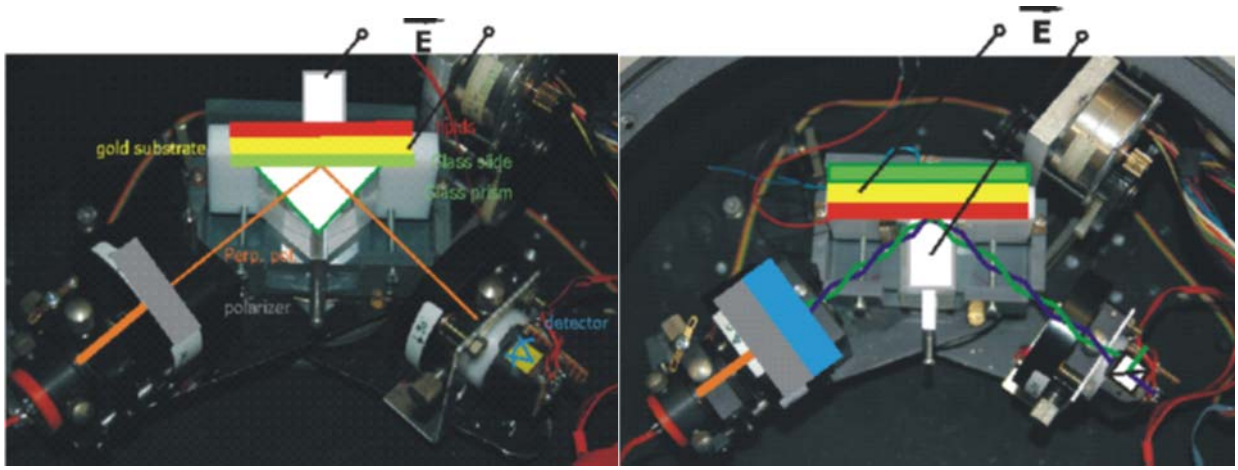

a b

Fig. 12. a) SPR spectrometer approach;
b) Ellipsometer: orange – light beam; gray – polarizator; blue – λ/4 –plate; green – glass slide; yellow – gold layer; red – bilayer;

The ellipsometer (Fig. 12) is based on the same goniometric head as the SPR. Only the measurement chamber was redesigned. In the case of SPR the light is totally reflected at the gold and creates plasmons which interact with the optical probes from the bilayer. In the ellipsometer the light first interacts with the chromophores and than is reflected by the gold surface. In both cases the gold layer is used as an electrode and as a support for the

bilayer.

For controlling and data acquisition a microcontroller system (ADμC 812, Analog Devices, Norwood, MA, USA) has been used. The incident angle of the laser to the sample has been varied using a step-motor with 200 steps/360º. To increase the accuracy a planetary gearbox (5:1) has been intercalated between the motor and the goniometric head cantilevers. This increased the resolution up to 1000 steps/deg.

The electric stimulus between the electrodes has been generated by an arbitrary function generator controlled by a microcontroller with a 12bit DAC (digital analog converter). The electrical and optical answers have been acquired by the 12 bit ADC (analog digital converter) from the microcontroller and transferred via serial interface to the host PC. All data processing was done in Matlab©.

The start/stop position was detected by means of a Hall sensor. In the case of ellipsometer the angle between the light source and the normal to the probe surface has been kept constant to a value of 65º to be further away from Brewster angle where only the perpendicular to the surface polarization is reflected.

4.3.2. Optical and electrical detectors

It is known that in the case of reversible membrane electroporation only a surface fraction of one percent is porated. To detect these small changes a sensible detector should be used. The electrical and optical parameters have been recorded simultaneously.

The voltage has been measured between an Ag/AgCl electrode (1 mm diameter chlorodized silver wire) in the electrolyte (10 mM KCl) and the gold surface which supports the bilayer.

The optical signal has been detected by an integrated detector TSL250R from TAOS Inc. Texas, USA with the spectral response presented in Fig.13.

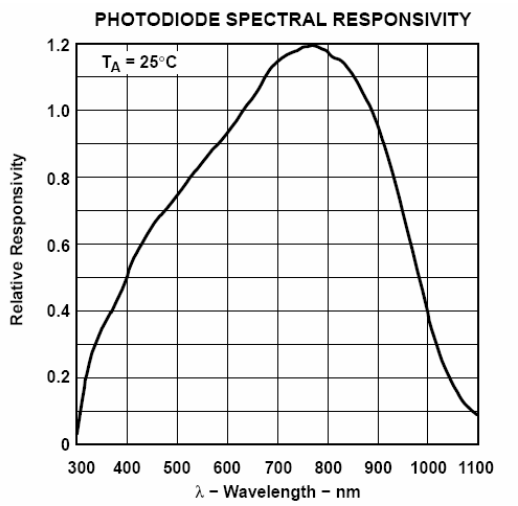

Fig. 13. The spectral response of the photodetector.

The active surface of the photodiode is 1 mm^2. The reasons to choose this detector are:
(i) highly integrated (photodiode, transimpedance amplifier, 16 MOhm feedback resistance, focusing lens) – all in one package;
(ii) linear response with the light intensity;
(iii) easy to interface with the data acquisition system.

4.3.3. Bilayers

All the bilayers has been made from POPC (1-Palmitoyl-2-Oleoyl-*sn*-Glycero-3-Phosphocholine – Avanti Polar Lipids, Alabaster, AL, USA) lipids used as delivered, solved in chloroform. The structure of POPC is presented in Fig. 14.

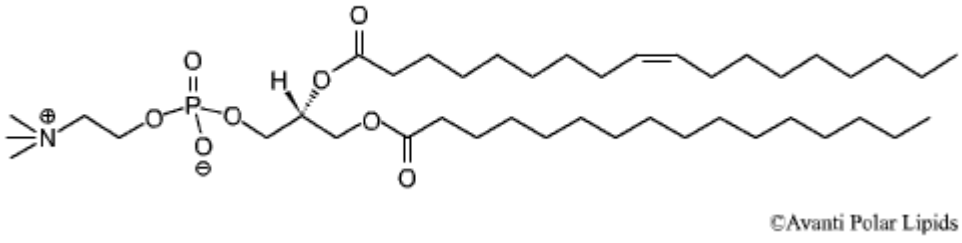

Fig. 14. POPC structure.

As optical probe for ellipsometry the BODIPY(581/591C_{11}) ((4,4-difluoro-5-(4-phenyl-1,3-butadienyl) -4-bora-3a,4a-diaza-*s*-indacene-3- undecanoic acid) – Invitrogen, Molecular Probes, Carlsbad, CA, USA) has been used. The optical probe (Fig. 15) has been solved in

methanol (1 mg/ml) as stock solution and stored in -20º C freezer.

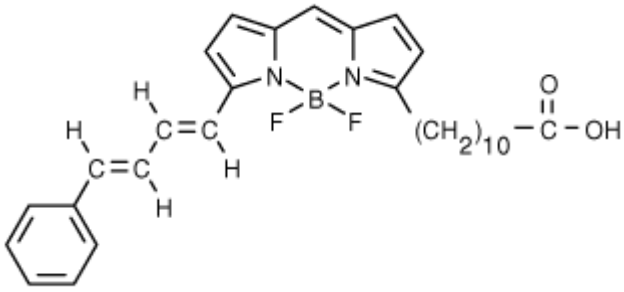

Fig. 15. BODIPY(581/591C_{11}) structure.

The investigated bilayers has been prepared using the gently hydratation methods described in the literature [12; 13; 14]. Briefly, the lipid solution (10 mg/ml) has been mixed with the optical probe (0,1 mg/ml) in different molar concentrations and spread onto the gold layer. Due to the small surface (40x35 mm), only a limited amount of solution (50µl) could be deposited without spill over. To reduce the evaporation rate the deposition has been made in a glass container partially filled with chloroform. The evaporation process takes 24 hours under a hood with the glass container partially open to allow a slow evaporation. After complete evaporation, the sample has been place in vacuum at about 10^{-3} mbar, for 24 hours, to completely evacuate the solvent molecules. The hydration took 24 hours and has been done in a glove box in the excess presence of water to insure that the humidity is 100%.

After hydration the sample has been mounted on the ellipsometer chamber, filled with electrolyte (10mM KCl) and the light intensity in the presence of the electric field measured.

The measurement chamber for types of investigation is showed in Fig. 16. On the glass surface, a 50 nm thick gold layer is deposed by physical vapor deposition method. On the gold surface the mixture lipid – chromophor is deposited and on top of the lipid layers a small electrode compartment is attached. The electrode compartment is made from Teflon© with glass windows and a 5 mm opening serving as a contact between electrolyte and sample. The maximum investigated surface is limited to the 1 mm diameter due to the focusing of the incident light. At the upper side of the chamber is a small opening for the Ag/AgCl electrode.

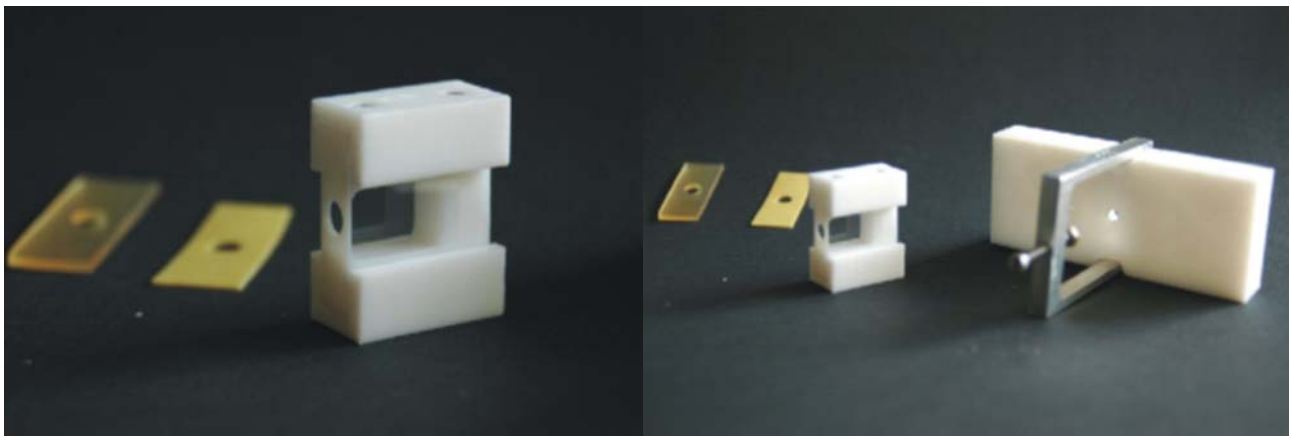

Fig. 16. Measurement chamber for ellipsomentrical and SPR investigations.

As support for bilayers a thin (50 nm) layer of gold on BK7 glass slides (index of refraction n_d = 1,5168 at 587,6nm), (gift from Dr. Renate Naumann, MPI Mainz, Germany) prepared using physical vapor deposition method has been used. After measurements the glass slides have been cleaned using, first ethanol 70% and second, a solution (1:3 v:v) of oxygenated water (H_2O_2 – 30%) and sulfuric acid (H_2SO_4 – 98%). The glass slides where stored in water and prior usage where dried using compressed nitrogen.

5. Results and discussions

The experimental data suggest the formation of highly oriented stacks of bilayers onto the gold surface. Comparing the data on the bare gold surface with the data in the presence of bilayers, it is seen that the intensity of the light of the two polarizations are changed dramatically.

In the case of SPR, only some approximations are possible. From literature [15], it is known that the degree of membrane electroporation is maximal 10^{-3} in the case of cells, and 10^{-2} in lipid vesicles. Using this assumption the reflectance was calculated (Fig. 17) using the following parameters: prism SF10 glass (n = 1,723), gold (d = 50 nm) and lipids layer (n = 1,45). Another assumption has been that, in the case of electroporation, maximally 1% of the lipid layer includes water molecules. The angle of minimal reflectance has changed by 0,15° (from 74,20° to 74,35°), thus the reflectance minimum decreases by 3,8% (from 0,2072 to 0,2110).

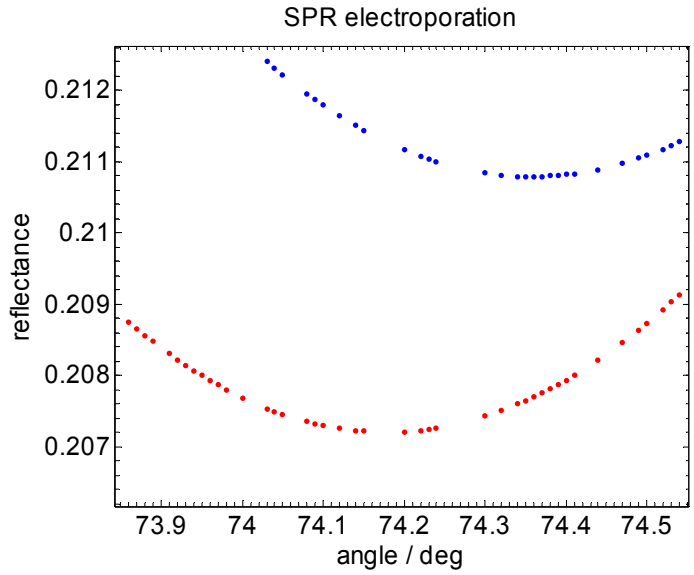

Fig. 17. Theoretical membrane electroporation. red – pure lipid layer; blue – lipid layer with 1% water molecules.

The refractive index of the membrane is calculated as:

$$n_{electro} = n_{lipid} \cdot 0,99 + n_{water} \cdot 0,01 . \quad (n_{electro} = 1,4488) \qquad (21)$$

The ellipsometrical approach supports that the formation of highly orientated stacks of bilayers was successful. In the presence of lipids, the sagittal (to the surface) polarization is zero because of the absorbance of the chromophor. However, also a part of the parallel polarization is absorbed probably due to a lost of orientation in the upper part of the stack.

An overview of the results is presented in the Fig. 19 and Fig. 20. For reference, a clean surface is measured to assured that the intensity of light polarization on both channels is as equal as possible (Fig. 21). Then, on the gold surface the lipid solution is pipette-ed and another measurement is done. From a mixture from 5µl BODIPY solution (1mg/ml) and 45µl POPC (10mg/ml), 1:60 ratio between BODIPY / POPC molecules, the results pointed that the signal from perpendicular polarization is zero and the signal from sagittal polarization is only one third from the parallel polarization of the bare gold (Fig. 22). In the case of a mixture 25µl BODIPY-25µl POPC, 1:7 ratio between BODIPY / POPC molecules, the parallel polarization signal is 1% of the corresponding signal from the control measurement (Fig. 23). In both cases the signal corresponding to the perpendicular polarization approaches zero.

In the BODIPY structure (Fig. 15), the chromophor is oriented along the molecule and absorbs energy when the orientation of the incoming radiation is in plane with the long

axis of the molecule. If the electric field vector of the incident light has another orientation than the transition dipolar moment of the chromophor, the absorbance decreases until it becomes perpendicular to the molecule plane when it is at a minimum level.

This can be the explanation of the zero intensity for the signal corresponding to the perpendicular polarization. However, also the signal corresponding to parallel polarization decreases. One explanation is in the construction of the lipid stack. The POPC lipid has a transition temperature of about -6°C [16].

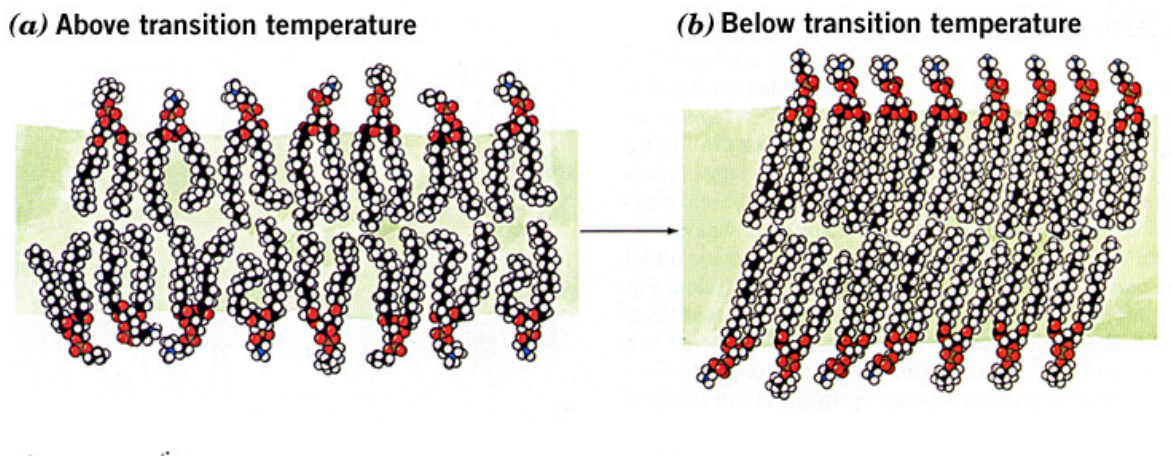

Fig. 18. Bilayer structure at different temperatures.

Above the transition temperature the structure is softer, the degree of orientation is far from perfect (Fig. 18), and the embedded chromophors move together so that the orientation of the optically active part is not perpendicular to the surface and the part of the energy form the parallel polarization is also absorbed.

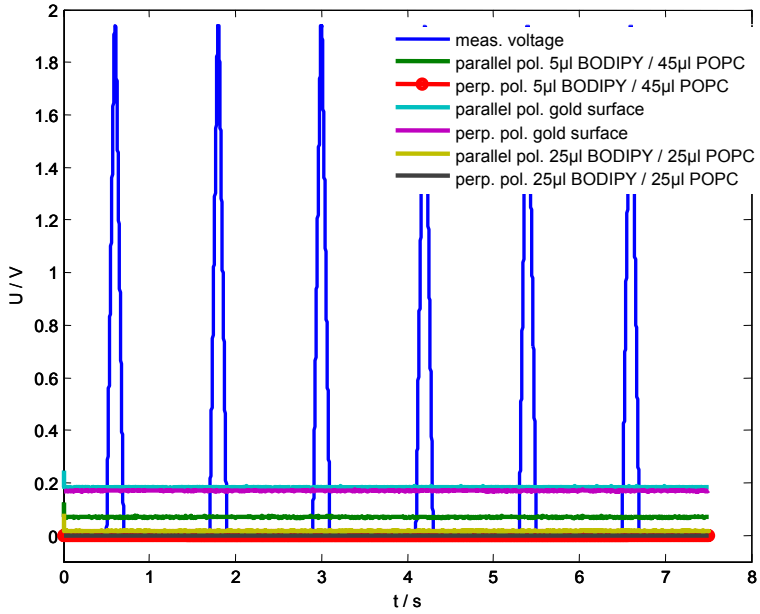

Fig. 19. Overview of the ellipsometrical measurements.

Another explanation for decreasing of the parallel polarization corresponding signal, is that the stack is well arranged for the first bilayers [17; 18] and that the disorder increase more and more until the top layer which can contain random orientated molecules.

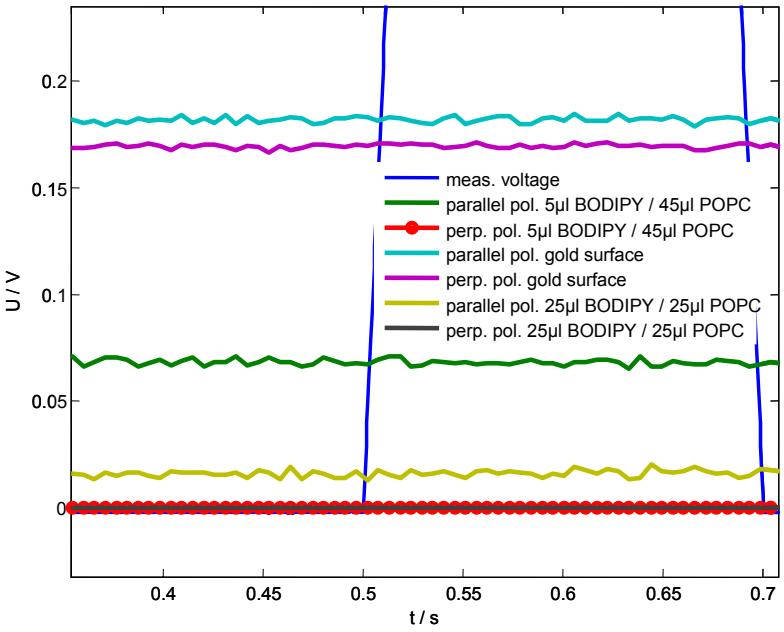

Fig. 20. Closer look at the ellipsometrical measurements.

The aim of this study has been the determination of the rotation degree of lipids in the electropores and this implies also an electric field across the stack of bilayers.

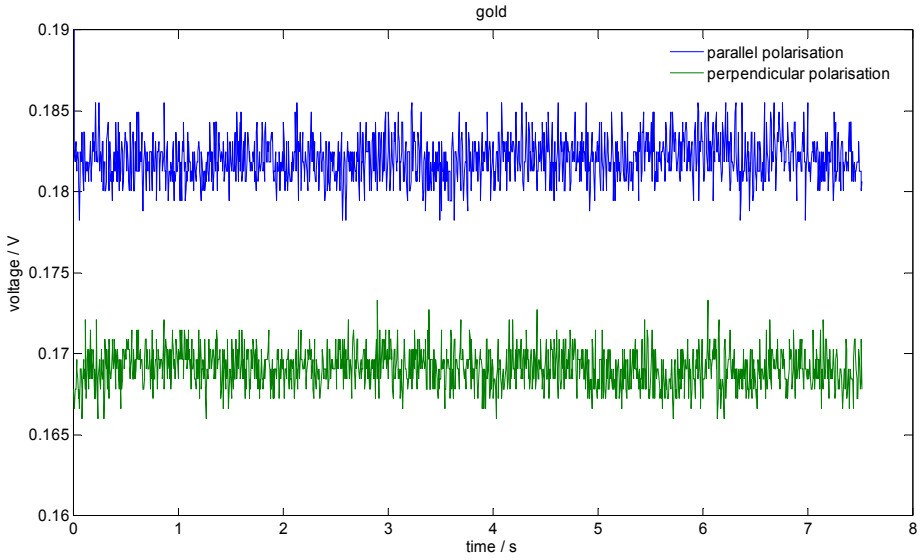

Fig. 21. Gold – water system response. The system has been adjusted so that the signals corresponding to the parallel and sagittal (to the surface) polarization to be as close as possible in order to have the same intensities. This is considered the reference measurement.

This means that the stack should have a continuous surface without defects, which becomes challenging in practice. The capacitance measurements showed a short-circuit which owes to the fact, that the stack surface is too large and thereby increasing the probability of defects. Another possibility is a defect at the edges of the mounted glass (Fig. 16.), shunting the membrane electrically.

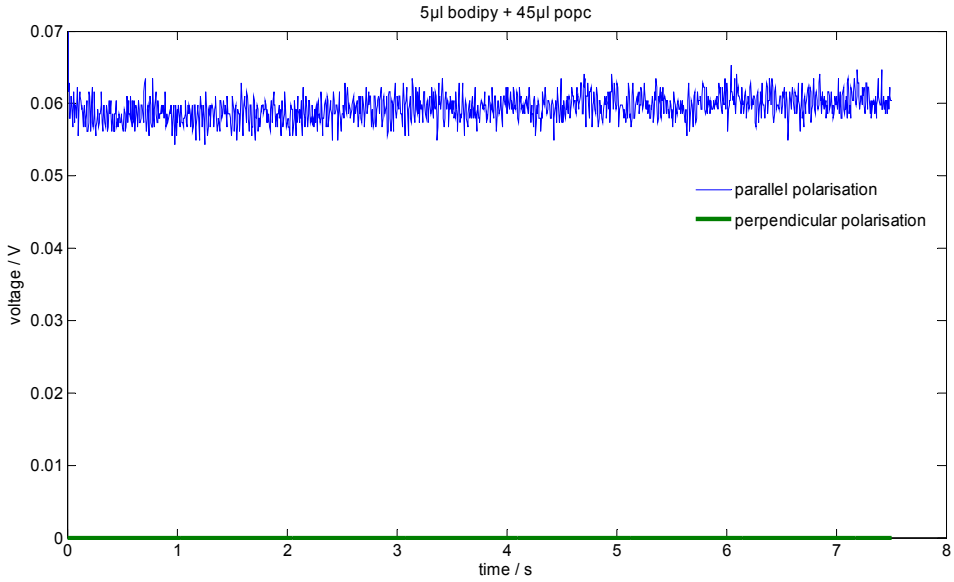

Fig. 22. 1:60 BODIPY-POPC molecular ratio stack of bilayers. The corresponding sagittal polarization signal is zero due to chromophor absorption. Also the signal corresponding to parallel polarization is smaller than the reference measurement (Fig. 21.) because the orientation degree of the bilayers decreases with the increasing distance from the gold surface.

The investigations to determine the degree of lipid rotation in the electroporation of artificial membranes where done using a "macro" approach. This means using a large surface and a high chromophor concentration.

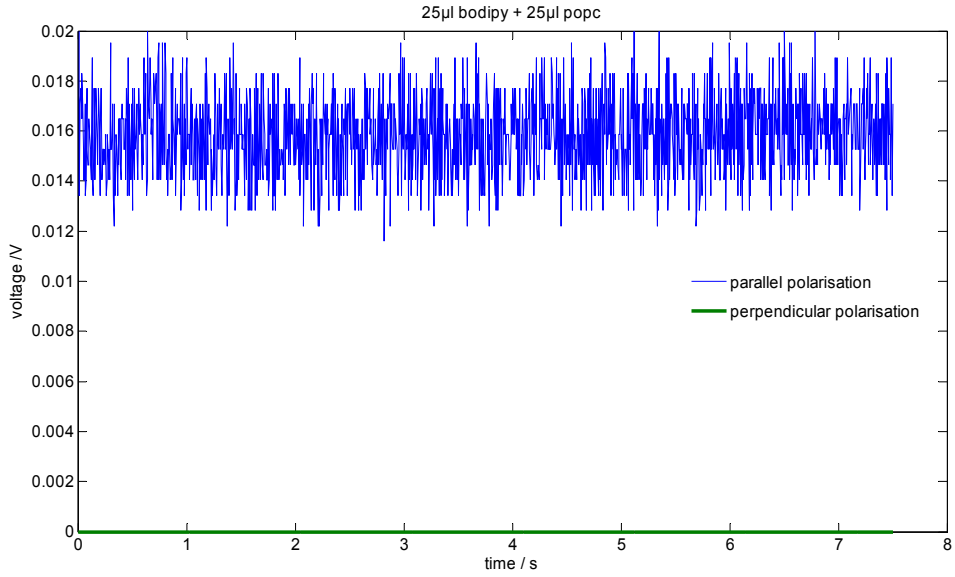

Fig. 23. 1:7 BODIPY-POPC molecular ratio stack of bilayers. The signal corresponding to parallel polarization is only one tenth of the reference signal. The sagittal polarized component of the signal is again zero.

The most crucial factor limiting the experimental outcome has been the low degree of electroporation (for spherical vesicles is maximum 1% [15]) and the detection unit which should have a high sensitivity to detect the maximally 1% changes within because permanently moving lipids. Since the electric field is the key parameter, the chamber should be constructed for application of a homogeneous field but still allowing the observation of the lipid layer for optical measurements.

A new direction worth to try is going to the "nano" scale looking to a single molecule, in the best case, or to a group of tens of molecules in the most probable way. One tool candidate can be SNOM – Scanning Near field Optical Microscopy. This microscope use an etched glass fiber, covert with aluminum on the lateral surface, with an tip opening in the tens/hundred of nanometers in diameter as a probe in a similar manner as an AFM – Atomic Force Microscopy [19]. Using the glass fiber this tool can illuminate a very small surface or can gather photons from a small surface of interest. It should be noted that the metallic surface from the glass fiber can be used as an electrode and the substrate material as the second electrode. The great advantage of this approach is that one can detect the chromophor at the same area as the field is applied. This would increase the intensity of the electric field only locally and could use a bilayer with defects. The drawbacks of this method are the need of a very sensitive optical detector and very high stability at parasitic mechanical vibrations.

6. References

[1] – E. Neumann, S. Kakorin, K. Tönsing, Fundamentals of electroporative delivery of drugs and genes, Bioelectrochemistry and Bioenergetics 48 (1999), p. 3-16

[2] – E. Neumann, Membrane electroporation and direct gene transfer, Bioelectrochemistry and Bioenergetics 28 (1992), p. 247-267

[3] – A. Gothelf, L.M. Mir, J. Gehl, Electrochemotherapy: results of cancer treatment using enhanced delivery of bleomycin by electroporation, Cancer Treatment Reviews 29(5), p. 371-387

[4] – R. Elez, A. Piiper, B. Kronenberger, M. Kock, M. Brendel, E. Hermann, U. Pliquett, E. Neumann, S. Zeuzem, Tumor regresion by combination antisense therapy against Plk1 and Bcl-2, Oncogene 22 (2003), p. 69-80

[5] – E. Neumann, S. Kakorin, Electroporation of curved lipid membranes in ionic strength gradients, Biophysical Chemistry 85 (2000), p. 249-271

[6] – U. Pliquett, R. Elez, A. Piiper, E. Neumann, Electroporation of subcutaneous mouse tumors by rectangular and trapezium high voltage pulses, Biochemistry 62 (2004), p. 83-93

[7] – E. Neumann, M. Schaefer-Ridder, Y. Wang and P. H. Hofschneider, Gene transfer into mouse lyoma cells by electroporation in high electric fields. *EMBO J.* 1 (1982), p. 841-845

[8] – W. Knoll, Interfaces and thin films as seen by bound electromagnetic waves, Annual Review of Physical Chemistry 49 (1998), p. 569-638

[9] – J.A. Woollam, B. Johs, C.M. Herzinger, J, Hilfiker, R. Syonowicki, C.L. Bungay, Overview of variable angle spectroscopic ellipsometer (VASE), Part I: Basic Theory and Typical Applications, Critical Reviews of Optical Science and Technology CR72, (1999)

[10] – J.A. Woollam, B. Johs, C.M. Herzinger, J, Hilfiker, R. Syonowicki, C.L. Bungay, Overview of variable angle spectroscopic ellipsometer (VASE), Part II: Advanced Applications, Critical Reviews of Optical Science and Technology CR72, (2000)

[11] – M. Yamamoto, Surface plasmon resonance (SPR) theory, Review of Polarography 48 (2002), p. 209-237

[12] – M. Seul, M.J. Sammon, Preparation of surfactant multilayer films on solid substrates by deposition

from organic solution, Thin Solid Films 185 (1990), p. 287-305

[13] – C.A. Keller, K. Glasmästar, V.P. Zhdanov, B. Kasemo, Formation of supported membranes from vesicles, Physical Review Letters 84 (2000), p. 5443-5446

[14] – S. Ludtke, K. He, H. Huang, Membrane thinning caused by Magainin 2, Biochemistry 34 (1995), p. 16764-16769

[15] – T. Griese, S. Kakorin, E. Neumann, Conductometric and electrooptic relaxation spectrometry of lipid vesicle electroporation at high fields, Physical Chemistry Chemical Physics 4 (2002), p. 1217-1227

[16] – K. Keough, How thin can glass be? New ideas, new approaches, Biophysical Journal 85 (2003), p. 2785-2786

[17] – T. Salditt, C. Li, A. Spaar, U. Mennicke, X-ray reflectivity of solid supported, multilamellar membranes, The European Physical Journal E 7 (2002), p. 105-116

[18] – C. Münster, J. Lu, S. Schinzel, B. Bechinger, T. Salditt, European Biophysical Journal 28 (2000), p. 683-688

[19] – G. Binning, C.F. Quate, Ch. Gerber, Atomic force microscope, Physical Review Letters 56 (1986), p. 930-933

Manuscript published in:

11. Heiligenstädter Kolloquium – Technische Systeme für Biotechnologie und Umwelt

Dieter Beckmann, Manfred Meister (Editors), 2002

ISBN 3-00-011287-1

Electroporation of single CHO cells

Catalin Gabriel Frantescu, Uwe Pliquett and Eberhard Neumann

Physical and Biophysical Chemistry, Faculty of Chemistry, University of Bielefeld, P.O. Box 100131, D-33615 Bielefeld, Germany

Key words: electroporation, single cells, patch-clamp, current-clamp, voltage/current characteristics

1. Introduction

A lipid membrane, artificial or natural, can become permeable by exposure to a brief high-intensity electric field pulse, causing membrane electroporation. In the electroporated state a lipid membrane is highly permeable to small ions and even macromolecules.
Electroporation is a commonly employed method for gene transfer and for the transport of other normally impermeant molecules into cells. Electroporation is a candidate method for enhancing drug delivery across the skin into organs. Further optimizations of application protocols require advanced investigations on the membrane level.
Besides the desired electrotransport, electroporation exhibits some side effects. For instance, Joule heating can diminish cell survival or even lead to irreversible damage.
The aim of this study is to characterize the electroporation process in term of different pore states.

2. Materials and Methods

CHO cells (chinese hamster ovary) are cultivated according to established protocols and harvested daily. They have been washed three times and resuspended in buffer (150mM KCl) or culture medium depending on the experimental needs. The microelectrodes are Ag/AgCl type electrodes, made from silver wire by chloridizing with 1M HCl electrolyte. The counter electrode is inserted into a 1mm glass capillary filled with 150 mM KCl and 5% agarose gel. The microelectrode is inserted into a glass pipette made from borosilicate glass PG120T-7.5 (HARVARD APARATUS LTD, UK). The pipettes have a tip opening of $1\pm0{,}5$ µm and an electrical resistance of $4\pm0{,}5$ MΩ. The microelectrode has been renewed for each single experiment in order to avoid artifacts due to impurities at the tip.

The electrical stimulus is generated by an arbitrary function generator and applied through a voltage-current converter. The stimulus and response signal are recorded with a computer attached to a 16 bit analog-digital converter. The microelectrode is positioned using a hydraulic micromanipulator (NARISIGHE, Japan).

The electrical setup is shown in Fig.1.

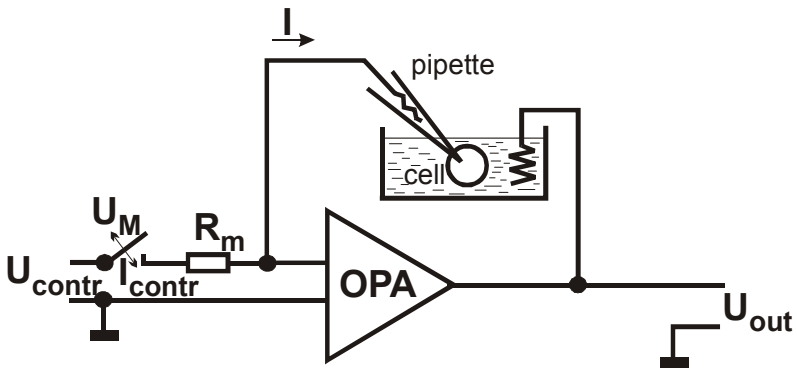

Fig.1 Experimental setup: either a current is injected (closed switch) or the transmembrane voltage is measured (open switch). The cell was attached in the whole-cell-clamp mode.

The voltage U_{contr} is provided by an arbitrary function generator with an resolution of 12 bit. When the switch is closed, a controlled current between -350 nA and + 350 nA is applied. In open position, U_{out} is just the transmembrane voltage. The offset correction is by a potentiometer and the junction potentials have been subtracted.

For compensation of the voltage drop across the pipette, we first record the response to a stimulus without the cell attached. Immediately after the cell is attached, a pulse of the same shape has been applied. The transmembrane voltage is obtained by subtraction of the voltage across the pipette from the recorded signal (Fig.2.). It is noted that, due to the current control the voltage across the pipette is the same with and without the attached cell.

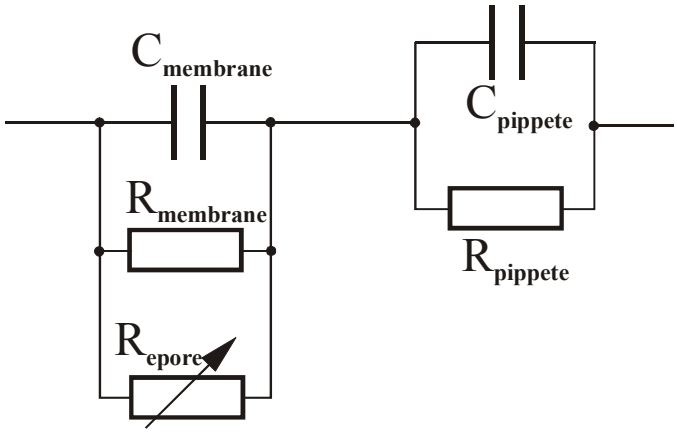

Fig. 2 Equivalent electric circuit of membrane and pipette.

The capacitive contributions (C_m) of the membrane have been subtracted using the theoretical ramp answer and the independently measured membrane impedance ($R_{membrane}$) . Due to the time required for electroporation, the critical voltage depends on the slope of the ramp. The critical voltage increases with increasing ramp velocity.

The observed nonlinearities in the U/I characteristics are not due to voltage gated channels because the plasma membrane of CHO-cells is not electrically excitable.

Experimentally, square pulses with t_{pulse} = 100 µs have been applied with amplitudes ranging from –300 nA – 0A (hyperpolarization) and from 0A up to 300 nA (depolarization) in steps of 50 nA. We exchanged the cell and the pipette for each experiment consisting of only one pulse.

3. Results and Discussion

The voltage U_M and current I at t = 100 µs have been used to assess the voltage/current characteristics of the plasma membrane of CHO-cells (Fig.3.).

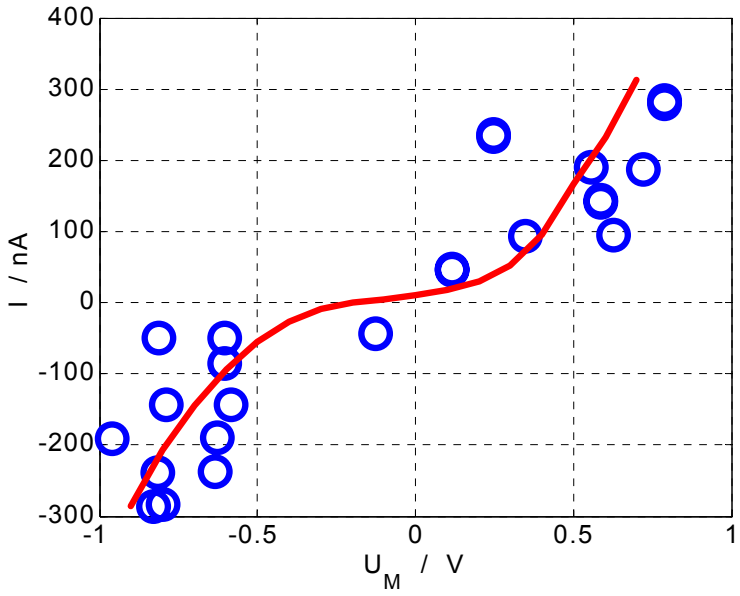

Fig. 3 Current / voltage characteristics of the plasma membrane of CHO-cells at the end of a 100 µs square pulse with controlled current.

An asymmetry at $\Delta U_M \approx$ -100 mV is observed. This value is interpreted as being due to the resting potential of the membrane as well as due to the asymmetric membrane structure resulting in different electroporation condition for the hyper- and depolarization side. At voltages exceeding 600 mV the second derivative of the current $\frac{d^2I}{(dU_M)^2} > 0$, is due to the decrease of the resistance R_{epore} of electropores (Fig.1.).

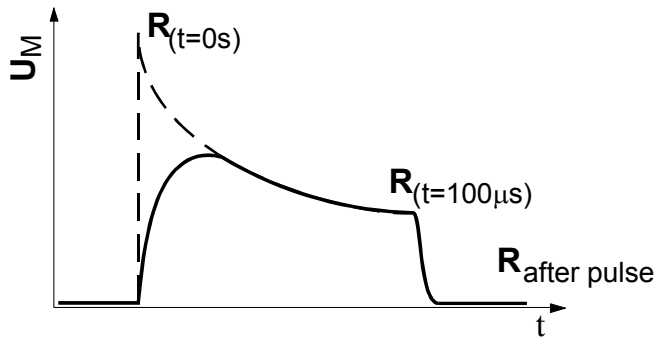

Fig. 4. Extrapolation of the transmembrane voltage to t=0s, for an ideal current step.

The U_M/t – dependence is estimated by $U_M = IR_p$ with

$R_p = (R_{t=0} - R_{t=\infty})\exp[-t/\sigma] + R_{t=\infty}$. $R_{t=0}$ is the resistance at the beginning of the pulse while $R_{t=\infty}$ is the resistance at $t \to \infty$. Note that $\sigma = C_M R_M$.

As shown in Fig.5. the voltage across the cell membrane does not decrease to U_M = 0V, despite a considerable drop in membrane resistance. The voltage due to a current exceeding 100 nA extrapolated to t = ∞ is decreasingly dependent on the current and levels off at U_M = 0.6 V.

The recovery of membrane resistance is different at different polarity (Tab.1.). The data are averaged over 24 experiments for each condition.

Table 1. Resistance at the beginning, the end, and 0.5 s after a pulse for depolarization and hyperpolarization conditions, respectively.

	I / nA	**$R_{t=0s}$ / MΩ**	**$R_{t=100\mu s}$ / MΩ**	**$R_{after\ pulse}$ / MΩ**
depolarization	+250	9.1 ± 2.6	5.8 ± 1.2	111 ± 49
hyperpolarization	-250	7.8 ± 1	5.2 ± 0.46	218 ± 123

The resistance after hyperpolarization recovers to a greater extent than after depolarization, while there is no significant difference during the elevated transmembrane voltage.

Fig.5. shows a typical result of the voltage/current characteristics of a single membrane using current ramps with different maximal current between –350 nA .. 350 nA.

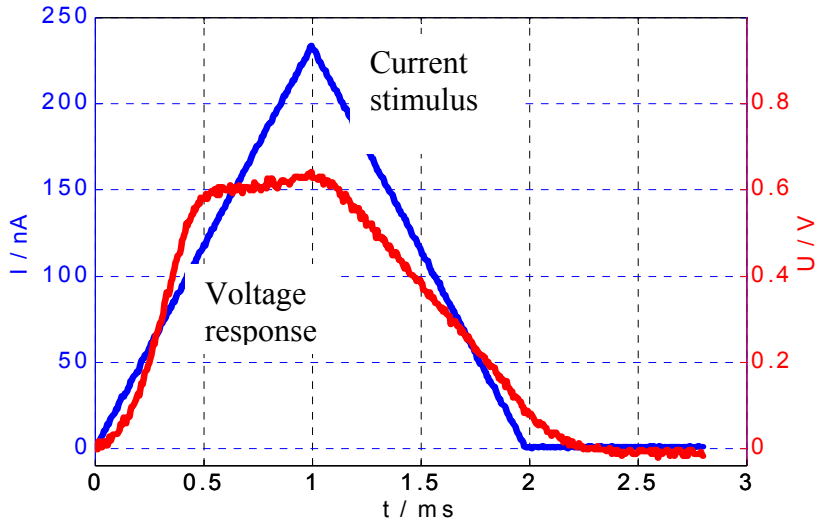

Fig. 5 Current triangle and voltage response of a CHO-plasma membrane as a function of time.

First the voltage rise is delayed due to the membrane capacity. The voltage then rises owing to the high resistance of the membrane. When the voltage reaches about 0.5 V it levels off and the membrane shows a voltage regulator effect, characterized by small changes of the voltage due to greater changes in current. At the falling edge, an almost linear behavior is found. The membrane is still partially charged at the end of the pulse. The transmembrane voltage finally reaches the resting potential of about –40 mV for CHO-cells.

From the difference of a linear response and the voltage measured one calculates the change in R_{epore} (Fig.1.), characterizing the extent of electroporation. The size of the newly created pores can be estimated form the voltage across the membrane. The pore radius is r_{epore} = 0.64 nm [Glaser et al.]. Since the pore conductivity (G_{pore} = 1,0 ± 0,5 pS) depends on r_{epore} , one can estimate the fractional surface $A_f = S_{pore}/S_{CHO}$, where S_{pore} is the surface of the electropores and S_{CHO} the total cell surface of the aqueous pathways. (Fig.6.)

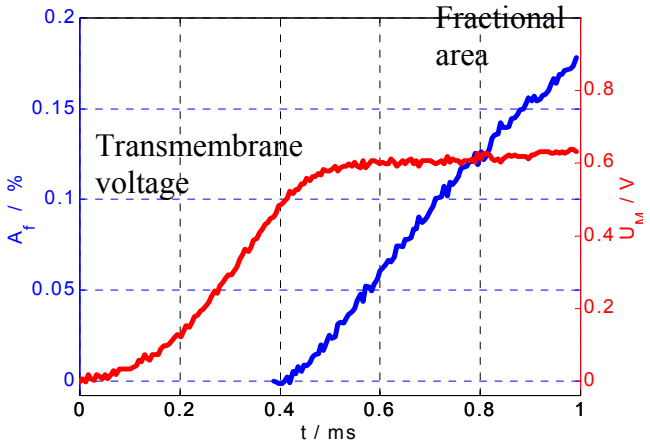

Fig. 6. Fractional area $A_f = S_{pore}/S_{CHO}$ of the newly created aqueous pathways and the transmembrane voltage as a function of the time t after the beginning of the pulse at t = 0.

In Fig.6. the process of pore creation appears to start at the transmembrane voltage U_M = 500 mV. U_M continues to increase with increasing current, yielding a nearly constant value of $U_M \approx 600$ mV.

Due to the extreme nonlinearity of the current/voltage characteristics at the rising edge and the almost linear behavior at the falling edge one can conclude a considerable difference in time by creating stabile pores and their resealing. The minimum scheme of pore creation requires at least 3 pore stages.

$$C \Leftrightarrow C^{*} \Leftrightarrow P \qquad (1)$$

where C is the closed state, C* is the prepore state and P is the open, conductive pore

state. Under electroporation condition the pores are created very fast (µs-range), while their resealing takes milliseconds up to minutes.

4. Conclusion

The use of whole clamp configuration for the investigation of electroporation on the membrane level offers the opportunity to separate hyperpolarization and depolarization effect. It is evident that the time of recovery as well as the resistance increase after an electrical stimulus depends on the polarity.

5. References

Neumann E, Sowers A, and Jordan C, Electroporation and Electrofusion in Cell Biology. Plenum Press, New York, 1989

Glaser RW, Leikin SL, Chernomordik LV, Pastuchenko VF, and Sokirko AI, Reversible electrical breakdown of lipid layers : Formation and evolution of pores. BBA 940: 275-287, 1988.

Manuscript published in:

11. Heiligenstädter Kolloquium – Technische Systeme für Biotechnologie und Umwelt

Dieter Beckmann, Manfred Meister (Editors), 2002

ISBN 3-00-011287-1

Unsymmetrische Elektroporation bei Depolarisation und Hyperpolarisation von CHO-Zellmembranen

Uwe Pliquett , Catalin Gabriel Frantescu and Eberhard Neumann

Physical and Biophysical Chemistry, Faculty of Chemistry, University of Bielefeld, P.O. Box 100131, D-33615 Bielefeld, Germany

Schlussel Wörter: Elektroporation, Einzellenzelle, patch-clamp, current-clamp, voltage/current characteristics

1. Abstrakt

Die Transmembranspannung von Zellen im Gewebeverband ist einer Messung über makroskopische äußere Elektroden nicht zugänglich, da sich die Spannungen über die jeweils gegenüberliegenden Seiten deer Zellmembran aufheben. Durch eine einseitige temporäre Permeabilisierung der Zellmembran summieren sich die Beiträge der entgegengesetzten Seite, wodurch an den Elektroden eine von der Struktur der Membran sowie der ionischen Kanäle und Pumpen abhängige Spannung gemessen werden kann. Es wird gefunden, dass die Membranelektroporation stark unsymmetrisch ist. Bei depolarisierenden Pulsen tritt die Elektropermeabilisierung im Bereich UM = 0.5±0.1 V auf, während bei hyperpolarisierenden Pulsen der Bereich UM = -0.95±0.15 V ist.

2. Einleitung

Die passiv-elektrischen Eigenschaften von Zellen im Gewebeverband lassen sich über Impedanzmessung ermitteln. Wenn äußere Elektroden mit Abmessungen im Zentimeterbereich verwendet werden, können nur Mittelwerte über eine große Anzahl von Zellen erhalten werden. Physiologische Parameter, wie Kanalaktivitäten oder die Zellmembranspannung lassen sich mit dieser Methode nicht erfassen. Durch Verwendung von Einzelzelltechniken, wie Whole-Cell-Clamp (Abb. 1) kann die polaritätsabhängige Antwort der Zellmembran auf einen elektrischen Stimulus oder direkt ihr aktiv elektrisches Verhalten gemessen werden. Außerdem ist die elektrische Feldstärke fast homogen über die Zellmembran verteilt, was besonders bei der Positionierung der Zelle zwischen zwei Elektroden nicht der Fall ist. Das aktiv-elektrische Verhalten der Zellmembran, besonders die Aktivität ionischer Kanäle, kann Auskunft über den Zustand der Gesamtzelle geben und ist geeignet, um die Entwicklung der Zelle innerhalb den nächsten Minuten oder Stunden nach einer Manipulation abzuschätzen.

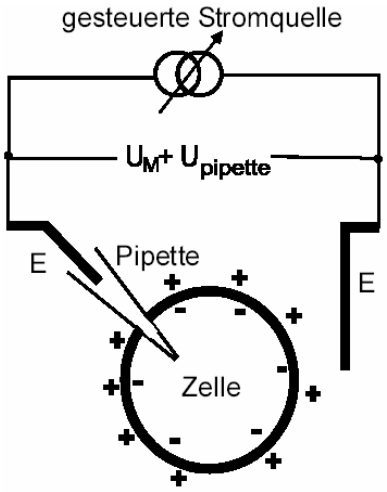

Abb. 1: Whole-Cell-Clamp-Anordnung für die Untersuchung der Hyperpolarisation bzw. Depolarisation von Zellmembranen. Die zwischen an der Pipettenspitze und der Pipettenelektrode abfallende Spannung wird durch Messung ohne die Zelle aber mit identischem Stimulus gemessen und anschließend zur Korrektur der Transmembranspannung verwendet. Die Elektroden E sind chlorierte Silberdrähte.

Der Schwerpunkt unseres Interesses ist das unsymmetrische nichtlineare Verhalten der Zellmembran. Ziel ist es, die Bedingungen für eine einseitige temporäre Permeabilisierung der Zellmembran zu finden. Damit kann man auch mit makroskopischen Elektrodenanordnungen zellphysiologische Eigenschaften messen, die ansonsten nur mittels Einzelzelluntersuchungen zugänglich sind.

3. Material und Methoden

Zellmaterial

CHO-Zellen (chinese hamster ovary) werden mit Standardmethoden gezüchtet und nach 3-maligem Waschen entsprechend dem Versuchsprotokoll in KCl-Puffer (140 mM) oder Kulturmedium resuspendiert. Für die Untersuchung werden nur nichtadhärente Zellen verwendet.

Pipetten

Die Pipetten zum Kontaktieren des Zellinneren wurden aus Borsilikatglas durch Ausziehen hergestellt. Der Durchmesser der Öffnung betrug etwa 1 µm. Ein chlorierter Silberdraht (ϕ = 0.5 mm) wurde als Elektrode verwendet. Bei einer Befüllung der Pipette mit 140 mM

KCl ergab sich ein Pipettenwiderstand zwischen 2 und 5 MΩ. Der Verschlusswiderstand (seal resistance) zwischen der Pipette und der Zellmembran liegt bei einigen 100 MΩ und spielt bei unseren Messungen eine untergeordnete Rolle, da der Widerstand der Gesamtmembran in der Größenordung von einigen MΩ liegt und somit erheblich kleiner ist.
Die Pipetten werden nur einmal verwendet, so dass das Experiment nicht durch Verunreinigungen der Pipette beeinflusst wird. Die Manipulation erfolgt über hydraulische Mikromanipulatoren (Narishige, Japan).

4. Verstärker

In allen Versuche wird eine Stromrampe von 70 µA/s appliziert und die über der Zellmembran abfallende Spannung gemessen. Ströme mit beliebiger Kurvenform werden durch eine spannungsgesteuerte Stromquelle mit 12 bit Auflösung und einem Maximalstrom von 350 nA generiert. Jede Pipette wird zunächst ohne Zelle gemessen. Da der Strom gesteuert wird, kann somit die an der Pipette abfallende Spannung genau bestimmt werden und anschließend zur Kompensation verwendet werden.

5. Resultate und Diskussion

Für Datenauswertung wird das Ruhepotential, UR, von der gemessenen Transmembranspannung abgezogen. Bei Spannungen von 0,5 V bis 0,7 V bei Depolarisation und von -0,8 bis -1,1V bei Hyperpolarisation beobachtet man einen rapidem Anstieg des Membranleitwertes. Der Betrag der Spannung sinkt trotz Stromanstieg ab. Danach bleibt die Spannung trotz Stromänderung weitgehend unverändert.

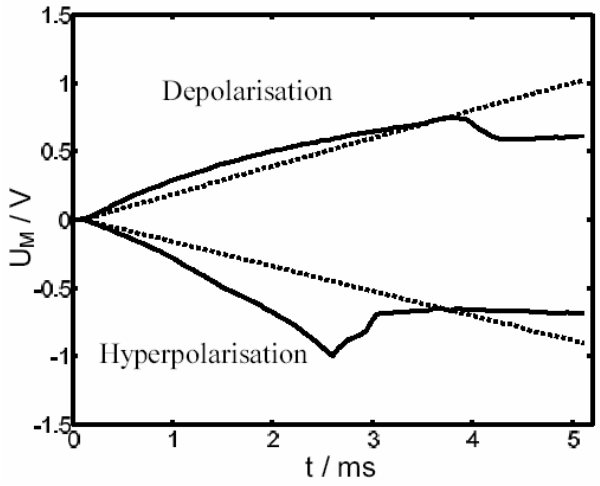

Abb. 2: Die Spannung UM (durgezogene Linie) als Funktion der Zeit als Antwort auf Stromrampen (gestrichelt) mit positiver und negativer Polarität. Depolarisation und Hyperpolarisation bezieht sich auf das negative Ruhepotential, UR, der Zelle.

Trägt man den Leitwert der Membranen, G = I/(UM-UR) auf, so findet man erhebliche Unterschiede bei De- und Hyperpolarisation (Abb. 3). Während der Leitwert bei Depolarisation leicht ansteigt, fällt er bei Hyperpolarisation zunächst ab bis Elektropoartion auftritt.

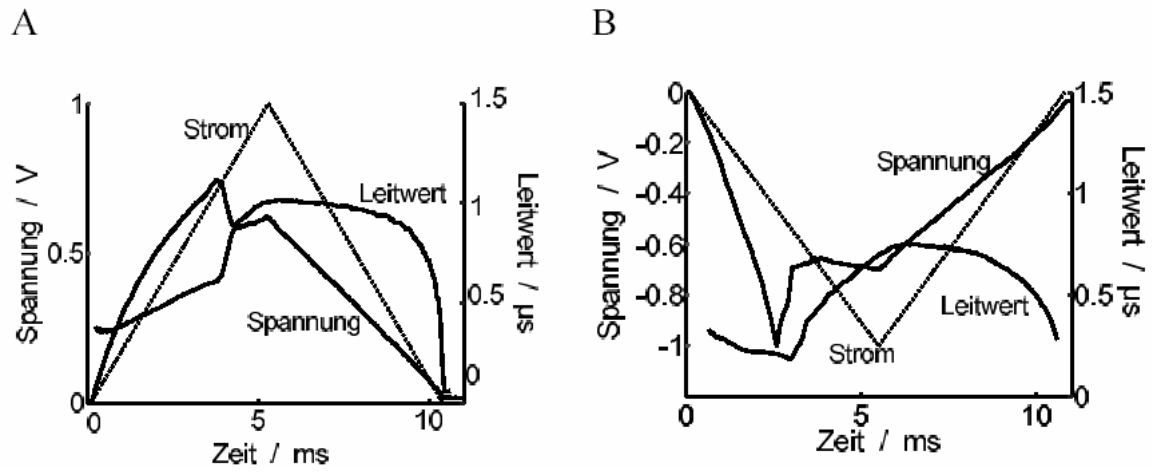

Abb. 3: Spannungsantwort der Zellmembran auf einen dreieckförmigen Stromstimulus bei (A) Depolarisation und (B) Hyperpolarisation. Der Leitwert G = (I/UM-UR), und wird damit geringfügig durch die auf der Membran akkumulierte Ladung verfälscht.

Durch die Verringerung der Leitfähigkeit auf der Hyperpolarisationsseite (Abb. 4) kommt

es dort zu einem schnelleren Anstieg der Transmembranspannung. Das bedingt, dass die Elektroporation im Zellverband auf dieser Seite früher erfolgt.

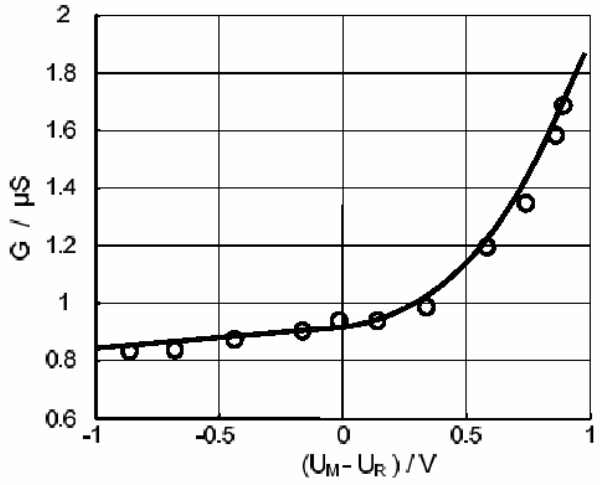

Abb. 4: Membranleitwert ohne Elektroporation in Abhängigkeit von der Transmembranspannung (UR subtrahiert). Die Daten (Kreise) sind über 92 Experimente gemittelt. Die Werte unterhalb von -0.6V und +0.4V sind extrapoliert.

Der Leitwert (Abb. 3) zeigt deutlich den Beginn des Anstiegsbereiches bei Erreichen der Elektroporationsbedingung. Ein weiterer Anstieg des Leitwertes führt zu einer Spannungsregulierung über der Zellmembran. Eine Verringerung des Stroms bewirkt nur eine leichte Verringerung des Leitwertes, wodurch sich auf der fallenden Flanke ein annähernd lineares Verhalten zwischen Strom und Spannung ergibt. Der Abfall des Leitwertes am Ende des Stimulus kommt hauptsächlich durch die Restspannung über der Membran zustande während der Strom bereits Null erreicht hat.

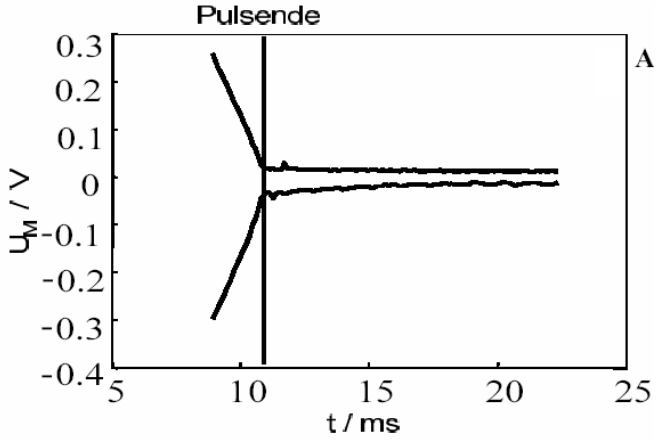

Abb. 5: Unterschiedliche Kinetik der Wiederherstellung der Transmembranspannung

nach De- und Hyperpolarisation.

Die Unterschiede bei Hyper- und Depolarisation sind der Schlüssel zur Messung physiologischer Eigenschaften der Zellmembranen wie der Transmembranspannung oder aktiver Ströme mittels makroskopischer Elektrodenanordnungen. Werden die Zellen eines biologischen Gewebes (oder Zellsuspension) einem Stimulus ausgesetzt, der zu einer einseitigen Permeabilisation führt, können die Eigenschaften der noch intakten Seite messtechnisch erfasst werden. Die hier verwendete Anordnung ist ein Hochspannungspulser (Scientiporator.), der nach Ablauf des Pulses hochohmig schaltet, so dass keine Stromumkehr an den Applikatorelektroden stattfindet (Abb. 6).

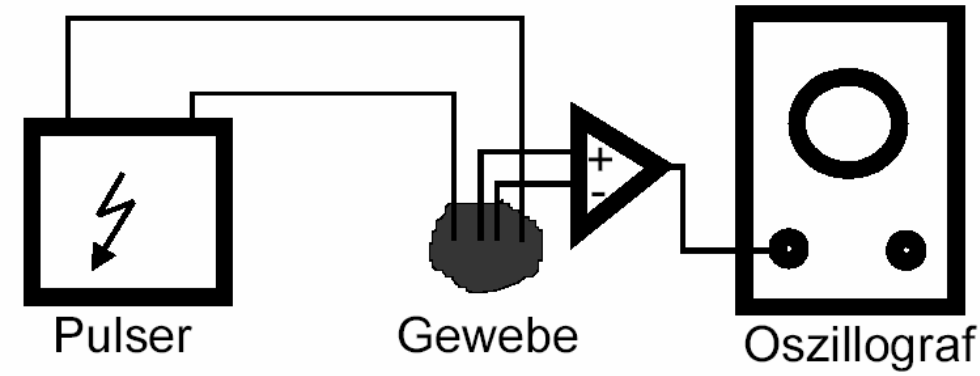

Abb. 6: Schema für die Applikation von Hochspannungspulsen an Geweben oder Zellsuspensionen mit Messung der Spannung. Der Pulsgenerator schaltet am Ende des Pulses hochohmig.

Ohne elektrische Stimulus heben sich die Transmembranspannungen der Zellen im Gewebe nach außen auf, so dass an den inneren Elektroden keine Spannung auftritt (Abb. 7).

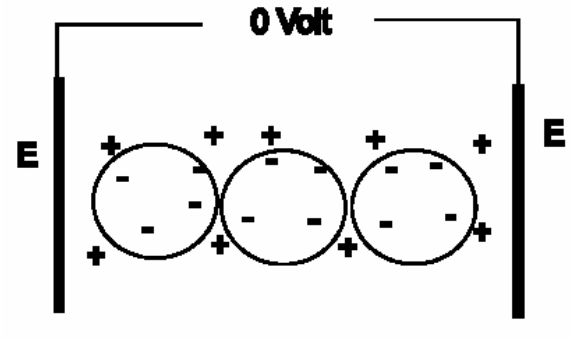

Abb. 7: Durch die Symmetrie der Zellen kann normalerweise keine Spannung an den

inneren Elektroden gemessen werden.

Durch Elektroporation werden die Zellmembranen permeabilisiert. Das Ruhepotential ist sofort nach dem Puls vernachlässigbar klein. Eine Restladung auf den Zellmembranen, hervorgerufen durch den elektrischen Stimulus hätte in jedem Fall die gleiche Polarität wie der Stimulus, da es durch den offenen Applikatorkreis zu keiner Stromumkehr kommen kann.

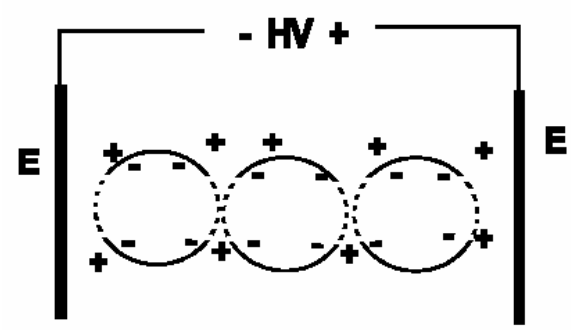

Abb. 8: Die Zellen werden durch Hochspannungsapplikation in den Polkappenbereichen transient permeabilisiert.

Überaschenderweise findet man nach der Elektroporation lebender Zellen eine in der Polarität dem Stimulus entgegengesetzte Spannung an den inneren Elektroden (Abb. 9).

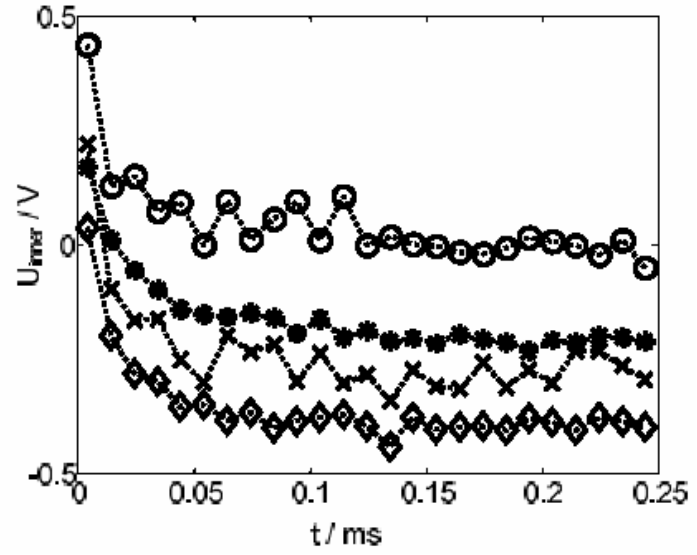

Abb. 9: Spannung zwischen den inneren Elektroden, Uinner, nach Abschalten eines positiven Rechteckpulses (800 V/cm) unterschiedlicher Pulsdauer über CHO-Pellets. Die

inneren Elektroden haben einen Abstand von 1mm. Die Pulsdauern waren: o 200 µs, x 400 µs, * 600 µs, . 800 µs.

Es wird angenommen, dass die Elektroporation an den beiden Polkappen unsymmetrisch ist. Die Wiederherstellung des ursprünglichen Membranwiderstandes auf beiden Seiten der Zelle weist eine unterschiedliche Kinetik auf. Die negative Spannung an den inneren Elektroden deutet auf eine nicht wiederhergestellte Hyperpolarisationsseite hin (Abb. 10).

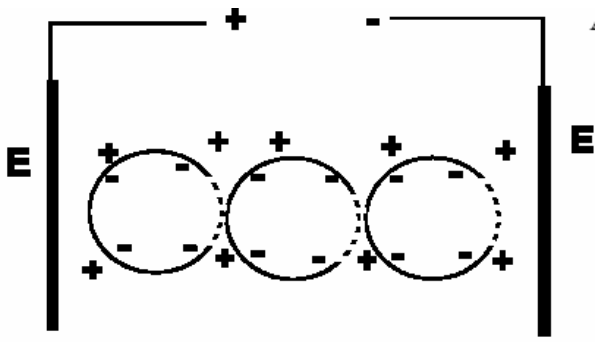

Abb. 10: Unsymmetrische Verteilung der Membranpermeabilität nach einem Hochspannungspuls. Bei permeabilisierter Hyperpolarisationsseite aber intakter Depolarisationsseite misst eine negative Nettospannung an den inneren Elektroden.

Die Abhängigkeit der Nettospannung von der Pulsdauer kann einerseits mit elektrochemischen Vorgängen auf der Membranebene, in deren Folge es zu einer Umverteilung der Ionen kommt, erklärt werden. Andererseits ist es wahrscheinlich, dass die Depolarisationsseite schneller wiederhergestellt wird als die Hyperpolarisationnseite. Da der Prozess der Wiederherstellung des Ruhepotentials der Zellmembranen hauptsächlich durch aktive Pumpvorgänge (Na+/K+ -Pumpe) bewerkstelligt wird, hängt die Kinetik der Wiederherstellung vom Zustand der Zelle sowie ihren Energiereserven ab. Die durch unsymmetrische Elektroporation hervorgerufene Nettospannung an den Sensorelektroden kann u.a. als quantitatives Maß für die Integrität der Zellen im Gewebeverband verwendet werden.

6. Zusammenfassung

Werden Zellen einem hohen elektrischen Feldpuls ausgesetzt, so kommt es zur

Elektroporation an den in Feldrichtung liegenden Polkappen der Zellen. Bei einer unsymmetrischen Elektroporation kann das Ruhepotential der Zellen ohne aufwendige Apparaturen (z.B. Patch-Clamp) gemessen werden.

Danksagung

Wir danken Marco Schmeer für hilfreiche Diskussionen, Thomas Seipp für die Bereitstellung der Zellen und der EU, Brüssel, für finanzielle Unterstützung (QLK3- CT-1999-00484, E.N.).

Manuscript published in:

12. Heiligenstädter Kolloquium – Technische Systeme für Biotechnologie und Umwelt

Dieter Beckmann, Manfred Meister (Editors), 2004

ISBN 3-00-015042-0

The membrane impedance before and after electroporation of single Chinese Hamster Ovary Cells

Catalin Gabriel Frantescu, Uwe Pliquett and Eberhard Neumann

Physical and Biophysical Chemistry, Faculty of Chemistry, University of Bielefeld, P.O. Box 100131, D-33615 Bielefeld, Germany

Key words: electroporation, single cells, patch-clamp, current-clamp, big electropores

1. Introduction

When exposed to electric field pulses, lipid bilayer membranes become permeable to ionic molecules and macromolecules, which usually can not pass the dielectric part of the membrane. This electric field effect is called membrane (MEP) electroporation. Nowadays, this field method is used for cell transfection with naked DNA [1]. Another powerful application of MEP is the enhancement of drug delivery especially for charged species [2; 3]. Although the mechanism of MEP is slowly being understood, the optimization of pulsing protocols still faces the problem of the only partially known electrical interactions of the external field pulse with the cell membranes.

Here, the electric resistance and capacitance of intact single cells are measured before and after electroporation. Since the field-induced structural changes in the membranes persist a long time after short-pulse electroporation (millisecond up to seconds), conventional impedance techniques in the frequency domain are not applicable. Therefore, we use a time domain approach monitoring the voltage change caused by rectangular current wave excitation.

The experiments are performed in the whole cell clamp configuration of selected single cells [4]. The advantages of this technique as compared to measurements in tissue or cell suspension are: (i) the access to a single membrane, (ii) the equally weighting of the entire membrane, no angle dependence and no averaging over membranes with arbitrary orientations, (iii) the application of depolarizing or hyperpolarizing pulses, with respect to the natural membrane potential, here $\Delta\varphi_{nat}$ = -60 ± 30 mV.

In the case of single cells, Joule heating is shown to be negligibly small.

2. Materials and Methods

Chinese hamster ovary (CHO) cells have been cultivated and harvested daily. Before use, the cells are washed in 150 mM KCI solution and resuspended either in 150 mM KCI solution or in culture medium, respectively. Reversible electrodes (Ag/AgCI) are used with one electrode inside the pipette contacting the cell. The pipette tip opening has a diameter

of Φ_p = 1 ± 0.5 µm and a resistance of R_p = 4 ± 0.5 MΩ. In order to avoid artifacts due to impurities at the tip, we renew the microelectrode für each single experiment with a single cello The attachment of the cell to the pipette and the manipulation of the cell is achieved by using a hydraulic micromanipulator (NARISIGHE, Japan).

The counter electrode is placed in a capillary filled with agarose (0.5 % by weight) in 150 mM KCI solution.

The electrical stimulus is generated by a computer-controlled arbitrary function generator and applied to the single cell through a voltage-current converter (Fig. 1).

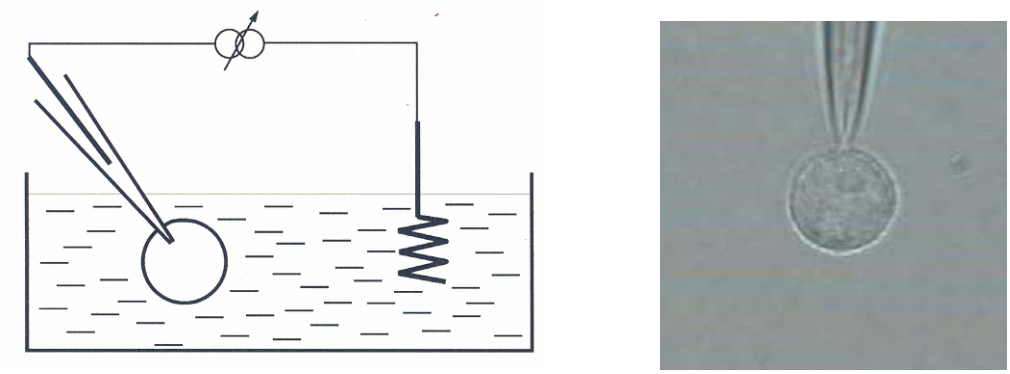

Fig.1 : Experimental setup. The cell is attached in the whole-cell-clamp mode.

The impedance measurements consist of 5 periods of a rectangular current wave of I_{imp} = 2 nA at a frequency f_{imp} = 10Hz prior to pulsing. After the pulse, a train of 35 to 40 periods are applied. The high field stimulus is either a triangle pulse or a rectangular pulse respectively.

The recorded voltage is the sum $U = U_p + U_m$ of the voltage across the pipette (U_p) and the transmembrane voltage (U_m). Moreover, the additional voltage, generated by liquid junction and, diffusion potentials, is processed as an offset.

Since we use a current stimulus, U_p is not dependent on the resistance (R_m) of the membrane. Therefore we are able to access the pipette voltage (U_p) separately, by measurement with no attached cell. For each experiment, a new pipette filled with

medium is used, and the voltage is recorded with the same protocol as in the case of the not attached cell. Subsequently, the experiment with the cell, is performed, yielding

$U=U_p+U_m$.

Therefore, each experiment yields two voltage/time traces (Fig. 2), the offset correction is performed by a differential amplifier prior to the experiments. Obviously, the membrane voltage is calculated according to

$U_m=U-U_p$.

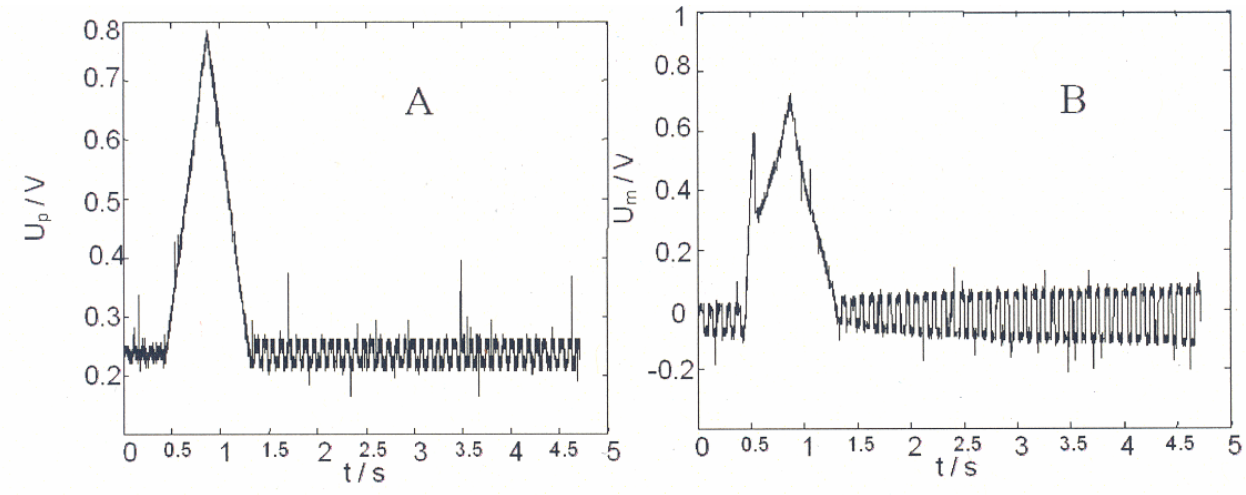

Fig. 2: Time courses of $U_p(t)$ and $U_m(t)$. (A) the pipette voltage (U_p) caused by a current stimulus without the attached cell. The calculated membrane voltage (U_m) as a function of time. For the experiment shown here, the current ramp is applied at t = 0.5 s, reaches the maximum at I = 150 nA at t = 0.9 s and returns to I = 0 at t =1.3 s.

The applied signal is superimposed to the. cell resting potential, defined as $\Delta\varphi_{nat} = \varphi_{in} - \varphi_{out}$, using the extracellular compartment as a reference with φ_{out} = 0 V. Note that $U_{nat} = \varphi_{nat}$. At hyperpolarization ofthe cell membrane, the potential φ_{in} of the cytoplasm (facing the pipette electrode) becomes more negative. The membrane is depolarized by increasing the potential φ_{in} up to $\varphi_{in} > 0$ (positive).

In brief, by selecting the polarity of the current stimulus we either hyperpolarize or depolarize the entire cell membrane with respect to the natural (resting) potential, here

$\Delta\varphi_{nat}$ = -60 ± 30 mV. Once the apparent threshold voltage U_{thr} for membrane electroporation is reached, a dramatic decrease in the membrane resistance R_m occurs. Due to the finite time required for electroporation, the threshold voltage depends on the slope of the ramp; increasing with increasing slope of the ramp.

3. Results and Discussion

Before application of the electroporation ramp the membrane impedance is calculated by fitting the positive edge of the rectangular voltage signal with an exponential function (Fig. 3). The charging time constant of the non-electroporated membrane is in the range 105 ≤ τ_m / s ≤ 141, where τ_m = $C_m R_m$. The membrane resistance R_m is calculated from the difference ΔU of the mean voltage $\overline{U_+}$ during the positive half wave, and of $\overline{U_-}$ of the negative half wave of the rectangular pulse train. The amplitude of the current steps is ΔI. Note that $R_m = \frac{\left(\overline{U_+} - \overline{U_-}\right)}{\Delta \cdot I}$.

The membrane capacity is given by C_m = τ_m IR_m.

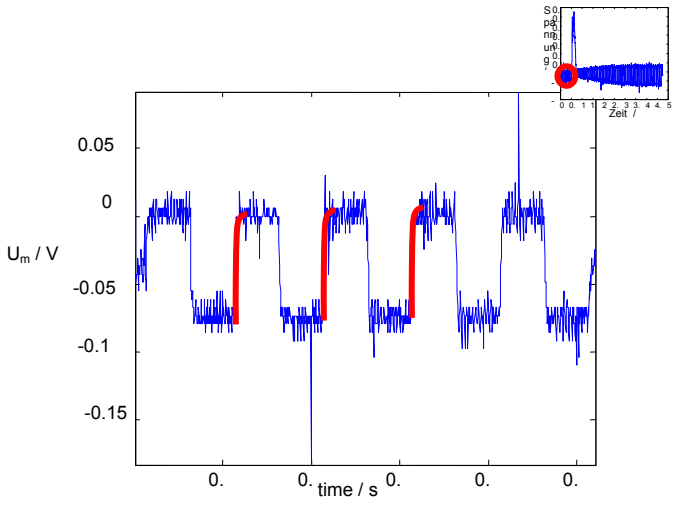

Fig.3: The membrane voltage U_m = $\Delta\varphi_m$ = φ_{in} -φ_{out} , induced by the applied train of rectangular current signals as a function of time, up to the time point t = 0.5 s. The rectangular current wave has the frequency of f =10 Hz.

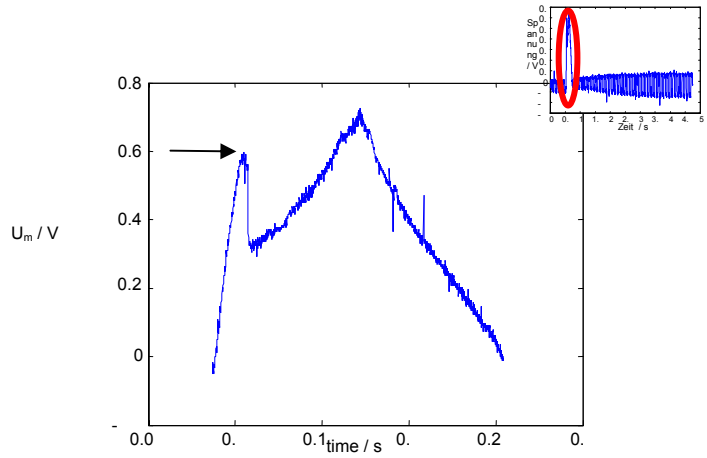

Fig.4: The induced membrane voltage U_m during a depolarisation current ramp as a function of time. The apparent electroporation threshold voltage here is $U_{thr,dep}$ = 0.6 ± 0.01 V (arrow). Ln the case of hyperpolarising ramps, the threshold voltage is $U_{thr,hyper}$ = -0.9 ± 0.01 V.

In order to induce membrane electroporation, a current ramp, varying in amplitude and slope, is applied to the plasma membrane. The sudden decrease in the transmembrane voltage, despite the further increase in the current, clearly indicates that aqueous pathways for ions are created in the lipid structure as a response to the increased membrane field (Fig. 4).

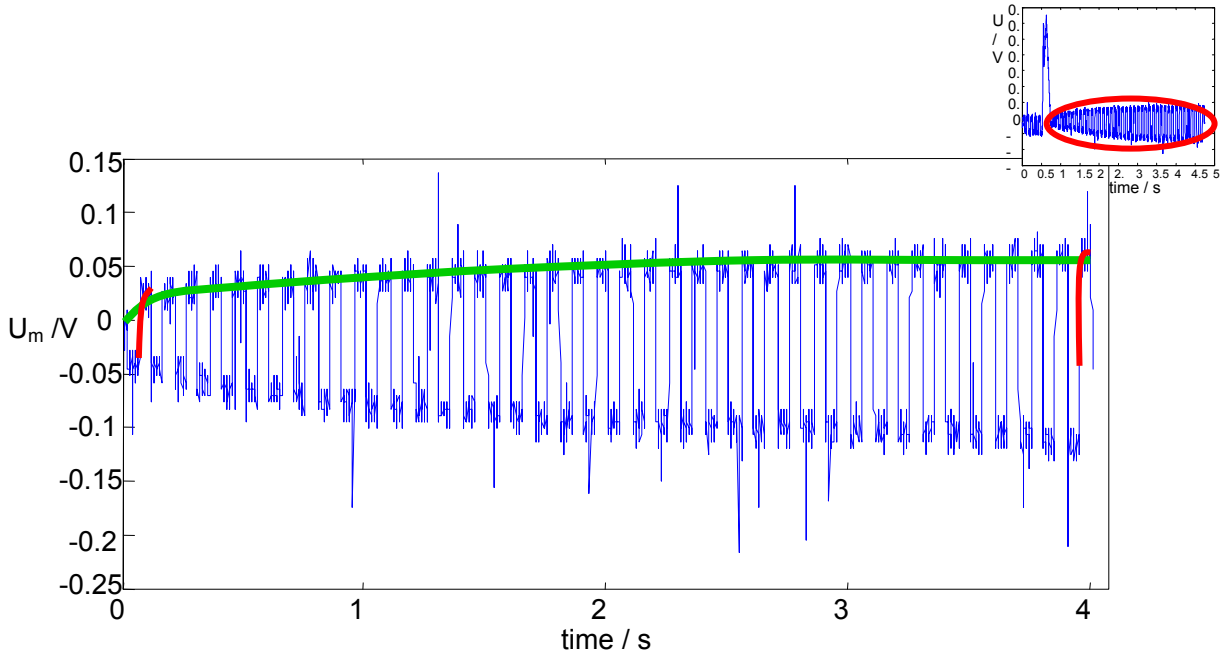

Fig. 5: The membrane voltage U_m induced by a rectangular current wave, as a function of time after electroporation of the single cell.

For data comparison between individual experiments, the specific resistance R_A and the specific membrane capacitance C_A are calculated, respectively, modeling the cell as a sphere. Note that $\tau_m = C_m R_m = R_A C_A$.

The radius is determined microscopically from a video stream (saved for further data processing).

In Fig, 5, it is shown that, after the current ramp, a post-pulse wave of rectangular current pulses is applied in order to calculate the membrane impedance during the recovery phase (Fig. 5) in terms of R_m and C_m.

It is found that indeed the resistance R_m ofthe plasma membrane recovers with the time constant $\tau_{rec} = 2 \pm 0.5$ s, as derived from both the resistance R_A (Fig. 6) and $U_m(t)$ (Fig. 7).

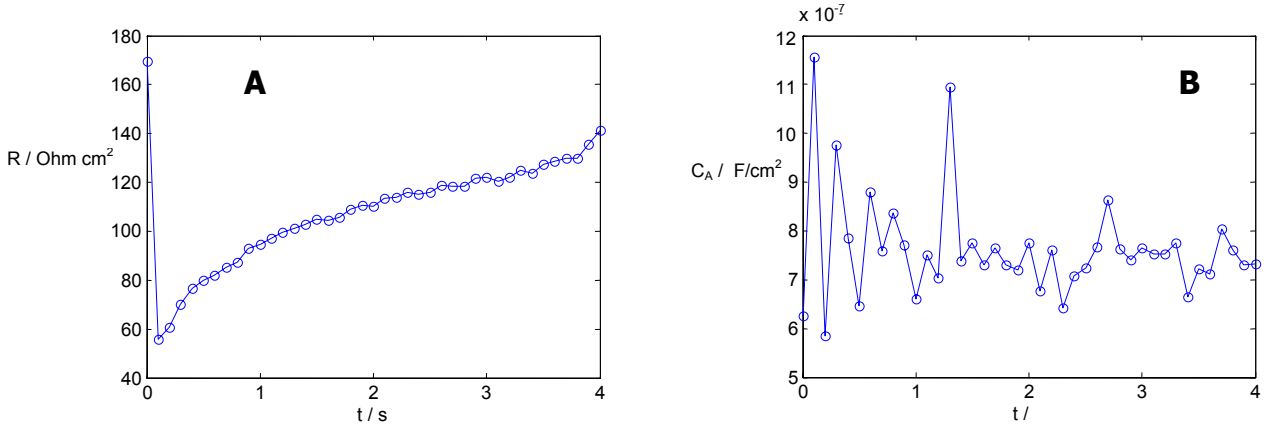

Fig. 6: The specific membrane resistance R_A (A) and the specific membrane capacitance C_A (B) both as a function of time.

Before the electroporative current ramp, $R_{A(before)} = 170\ \Omega cm^2$. After the ramp, R_A recovers within 4.5 s to the stationary value $R_{A(after)} = 100\ \Omega cm^2$. There are no significant changes in C_A due to membrane electroporation. Before the current ramp, $C_{m(before)} = 0.83\ \mu F/cm^2$, immediately after electroporation $C_{m(after)} = 0.79\ \mu F/cm^2$ and after 4.5 s we have $C_{m4,5s} = 0{,}75\ \mu F/cm^2$.

As seen in Fig. 6, Um decreases with time after electroporation, probably due to resealing of the electropores. The recovery of the transmembrane voltage is consistent with ongoing recovery of the membrane resistance (Fig. 7).

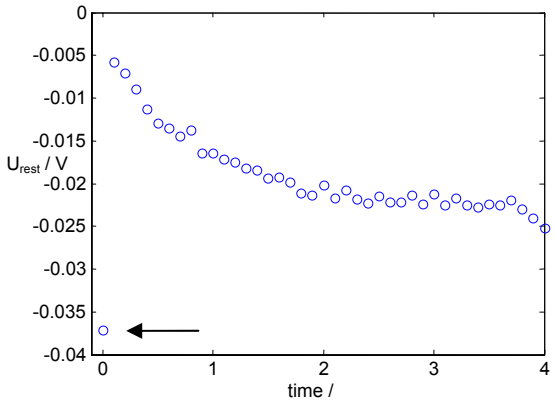

Fig.7: The membrane voltage U_m before (arrow at -37 mV) and after a depolarizing ramp pulse of duration 1 s, as a function of time (recovery phase).

As judged from the microscopic phase contrast images in Fig. 8, there are apparently no visible damage of the cells 5 s after electroporation (Fig. 8). However, video microscopy reveals that there is some disintegration of the membrane, if a current pulse exceeding for instance 200 nA hag been applied for one second. In such case protruding blebs and smaller vesicles develop at the cell surface. Finally the cell appears damaged within several seconds after the 200 nA / 1 s -pulse.

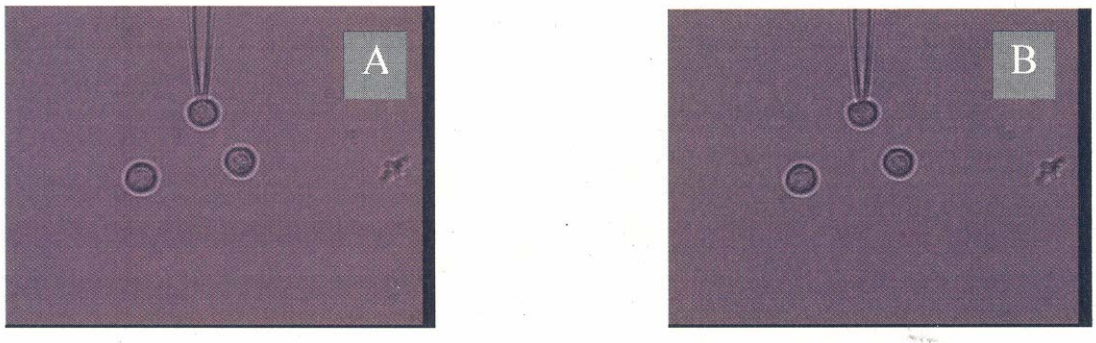

Fig.8: Phase contrast visualization of the CHO cells before a pulse (A) and 4.5 s after the pulsing (B).

However, at moderate currents (50 nA) lasting less than a second, a striking result are distinct steps in the voltage as a function of time. The steps appear to reflect steps of electroporation leading first to a larger number of small pores with a radius of 1 nm. Some of the small pores appear to enlarge yielding pores up to a radius of 50 nm.

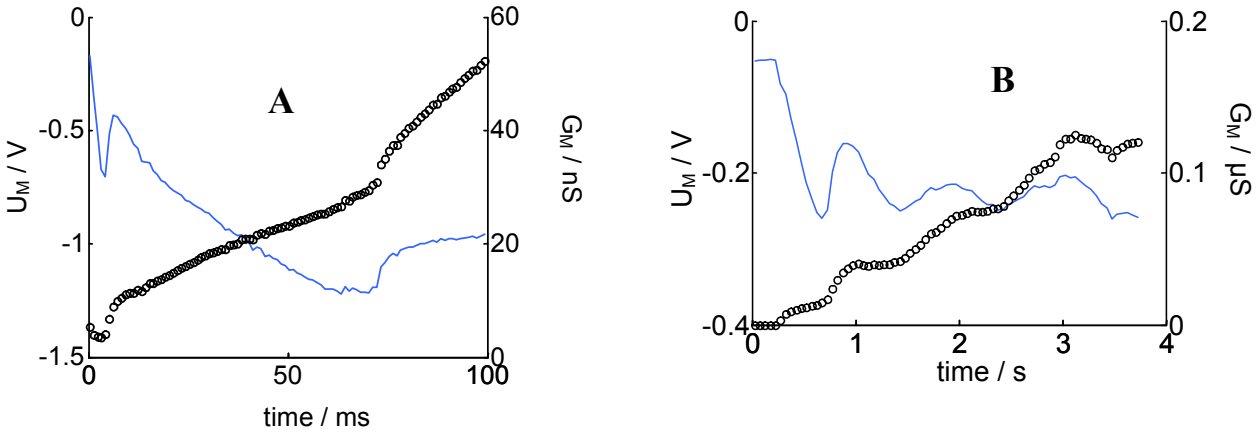

Fig.9: The membrane voltage $U_m(t)$ (solid curve) and the membrane conductance, $G_m(t) = I / U_m(t)$ (circles) due to a hyperpolarizing current ramp from 0 to -50 nA with ramp slope (A) -50 µA/s for t = 100 ms and (B) -12.5 nA/s for t = 4s.

If there are such big pores, it is not clear how they develop from initially small pores. Since the cell membrane is intracellularly supported by parts of the cytoskeleton, the electroporative stress and strain may extend to the cell interior and subsequently feed back to microscopic areas of the cell membrane. Thus, a pore within a stressed region may become the origin of a larger pore which, in turn, is limited in size by the intracellular structure of the cell. It is also feasible that localized electroporated areas are the origin of bleb formation and vesiculation.

4. Conclusion

The data indicate that also the plasma membrane of a single cell can be electroporated by current pulses. At moderate voltage and duration of the pulse, the changes are reversible and the cell membrane recovers to its value of the initial membrane resistance. The recovery of the membrane integrity takes several seconds, however cell survival is highly probable. The data can be analyzed in terms of two types of pores: small pores of radius

0.5 nm -1.5 nm and larger pores of 15 nm -50 nm. The results show that the current/voltage characteristics of the plasma membrane of a single cell can be determined by the whole-cell clamp technique.

5. References

1. Neumann E, Schaefer-Ridder M, Wang Y, and Hofschneider PR, Gene transfer into mouse lyoma cells by electroporation in high electric fields. EMBO J. 1: 841-845, 1982.

2. Mir LM, Orlowski S, Belehradek J, Teissie J, Rols MP, Sersa G, Miklavcic D, Gilbert R, and Heller R, Biomedical applications of electric pulses with special emphasis on antitumor electrochemotherapy, Bioelecttochem.Bioenerg. 38: 203-207, 1995.

3. Prausnitz MR, Bose VG, Langer R, and Weaver JC, Electroporation of mammalian skin: a mechanism to enhance transdermal drug delivery. Proc.Natl.Acad.Sci.(USA) 90: 10504-10508, 1993.

4. Frantescu CG, Pliquett U, and Neumann E, Electroporation of single CHO cells. In: Technische Systeme fur Biotechnologie und Umwelt,(Eds. Beckmann D and Meister M), pp. 543-549. Institut fiir Bioprozess- und Analysenmesstechnik, Heilbad Heiligenstadt, 2002, ISBN 3-00-011287-1

Acknowledgement

We thank Thomas Seipp and Ina Ehring for help in the cell culture work. We gratefully acknowledge the financial support of the ministry MSWF of the land NRW, grant Elminos and of the EU, grant QLK-CT-1999-00484 to E.N.

Manuscript published in:

IFMBE Proc. 2005 11(1)

ISSN: 1727-1983

ASYMMETRIC CHANGES IN MEMBRANE CONDUCTANCE DUE TO HYPER- AND DEPOLARIZATION: PROBING WITH CURRENT AND VOLTAGE CLAMP

U.Pliquett*, H.Krassen, G.Frantescu**, D.Wesner**, E.Neumann** and K.Schoenbach***

* Center for Biolelectrics, Old Dominion University, Norfolk, USA

** University of Bielefeld, Biophysical and Physical Chemistry, Bielefeld, Germany

Key words: electroporation, single cells, patch-clamp, current-clamp, voltage-clamp single pores

Abstract

Cell membranes are composed differently at the cytosolic and the extracellular side. This has a strong effect on the current-voltagecharacteristics (CVC) even if voltage gated channels are ignored. While a decrease of the conductance for small superimposed transmembrane voltages (<0.5 V) was found when chinese hamster ovary cells (CHO)–cells with no excitable plasma membrane hyperpolarized, the conductance rose as soon as a depolarizing voltage was applied. At higher voltage, both hyper- and depolarized membranes showed electroporation, but at different thresholds. Probing the CVC with controlled current or controlled voltage yields quite different results because of the variable voltage divider between the membrane and the electrolytes, which yields a positive feedback for voltage clamp condition but a negative feedback under current clamp condition. This also influences the results of pulsed field experiments in low (negative feedback) and highly conductive (positive feedback) media, indicating, for instance, a lower electroporation threshold of cells in tissues.

Introduction

The asymmetry in the electrical response of membranes at anodic and cathodic sides of cells in an imposed electric field was first observed by Hibino and coworkers [1]. Their explanation was that the superimposed electric field from the resting transmembrane potential increases the field strength at the anodic side while weakening it at the cathodic side. Thus, electroporation conditions are reached first at the anodic side. Under physiological conditions, the interior of a cell is negatively charged with respect to the surrounding medium. The transmembrane potential difference of a resting cell is usually between -50 and -90 mV, and depends on the cell type, the surrounding medium and the physiological state. A stimulus, lowering the potential inside the cell hyperpolarizes the membrane, while any increase of the intracellular potential causes depolarization. Even if the cell membrane is recharged with reversed polarity, it is still considered depolarization.
Using whole-cell-clamp conditions, it is possible to obtain hyper- and depolarization selectively at cell membranes. Current or voltage-clamp measurements provide quite different results in the sense that a current-clamp appears less destructive to membrane structures because the field strength increases only slightly after a critical level is reached (voltage regulator effect) [2]. In the case of a voltage clamp, the potential difference at the membrane is clamped, and thus, if the conductance of the membrane increases, a

current rise results with no regulatory feedback, i.e. the electric field causing the conductance increase remains unaffected. Consequently, the conductivity of the suspension medium has a great impact in electroporation studies. A high conductivity corresponds to voltage clamp, while a low conductivity provides current clamp. It implies that with the same field strength applied, the effect of electroporation is higher in a highly conductive medium.

Material and Methods

Whole cell clamp Glass capillaries (PG120T-7.5 HARVARD Part No. 30-0091) as well as borosilicate glass capillaries (GC120T-7.5 HARVARD Part No.30-0049) have been used to clamp the cell (Fig.1).

They have been pulled to a diameter between 1 and 3 µm using a DMZ-Universal Microelectrode Puller (Zeitz, Munich, Germany). The pipettes have been filled either with 140 mM KCl or culture medium. In both cases, the pipette had a resistance between 2 and 3.5 MΩ. The pipette was fixed at one wall of the acrylic measurement chamber and had an incorporated Ag/AgCl – electrode. The reservoir of the chamber was filled with culture medium. A liquid flow into the pipette was initiated by carefully reducing the pressure. Once the cell attaches to the tip, an electrical connection between cytosol and the electrode is established by breaking the cell membrane inside the pipette. The procedure of cell attachment was monitored by video microscopy (63 x, phase contrast, water immersion objective) and verified by impedance measurement of the cell membrane. Since the chamber is not temperature controlled, the experiments are conducted at room temperature.

Figure 1: CHO-cell sucked onto a capillary. The diameter of the cell is 14 µm.

The counter electrode (Ag/AgCl in 3 M KCL-agar), was in contact with the surrounding medium. An electric source (Fig.2) (voltage or current source) is controlled by a microcontroller-based arbitrary function generator. Current or voltage control is determined by getting feedback from either the current through the pipette or the voltage across the membrane.

The membrane voltage is acquired at the output of a compensation circuit, subtracting the pipette voltage from the voltage measured across the pipette and cell membrane. This compensation has to be adjusted before each experiment. In order to compensate for the pipette voltage under current clamp conditions, an identical measurement is made for the pipette without the cell attached. Since the current density is the same, the voltage across the pipette can be subtracted yielding only the membrane voltage. The offset arising from the equipment is adjusted to zero while the liquid junction potentials were corrected using the generalized Henderson equation.

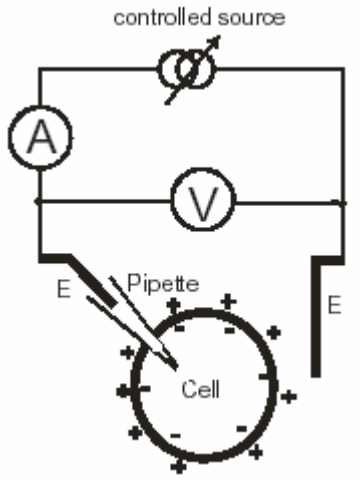

Figure 2: Schematic for the electrical connection of the cell.

Arbitrary function generator. This device generates any waveform with a temporal resolution of 500 µs for 10 s. A higher time resolution was possible by decreasing the total time, or vice versa, since the microcontroller had only 64 kB of memory. The bandwidth of the entire system including the pipette is on the order of 10 kHz. Depending on the feedback, either the voltage across the membrane or the total current is controlled with 12 bit resolution. The applied voltage is in the range $-10 \leq U/V \leq +10$; the current is controlled in the range $-350 \leq I/nA \leq +350$. Decreasing the feedback gain yields a higher

resolution, but lower output swing. Both the total current and the voltage
across the pipette are monitored with 12 bit resolution. The head stage with the matching amplifier is mounted onto the microscope which has been placed in a Faraday cage for electric shielding. The basic unit is a desktop device, connected to a PC via RS232. The microscope with the head stage is mounted on a granite plate for acoustic damping. While the PC programming was done in C++ for the driver and MATLAB for the user interface, the device itself is programmed in ASSEMBLER for efficient program execution. The highly automated processing of the video sequences is programmed in MATLAB.

Pulse protocols. Depending on the aim of the experiment, we adjust the pulse shape. For instance, the CVC of the plasma membrane of a single cell is derived from the response to ramp functions.

Rectangular pulses are applied when we study the relaxation kinetic parameters at a constant membrane field. Prior to, and immediately after the stimulus, we apply a rectangular wave with a repetition frequency of 100 Hz with low amplitude (i.e. ± 3 nA) in order to assess the impedance of the membrane by time domain spectroscopy. The measurements before and after the electrical stimulus also yielded the trans-membrane voltage (current clamp) or the short circuit current of the membrane (voltage clamp).

Cell preparation. Chinese Hamster Ovary cells (CHO) are used throughout our experiments. The culture medium (DMEM/F12) contained 5% FCS as well as 10-100 mg/L antibiotics like benzyl penicillin and streptomycin sulphate. The incubator was maintained at 37ºC (310 K) and a CO2-level of 5%. Since we conduct single cell measurements, they are highly diluted to prevent cell-cell interactions. CHO cells do not have excitable membranes, thus no precaution is taken to block voltage gated Na+ and K+ channels.

Video microscopy. All experiments have been monitored by a video equipped microscope. The videostream has been stored, together with the horizontal synchronization signal and the electrical stimulus using the audio channels (left, right) of the computer. The use of the synchronization signal made it simple to process the frames automatically using MATLAB.

Each cell was examined at the end of the pulse for negligible changes during the electrical stimulus. If the preset value of discrepancy was exceeded, the experiment was marked as suspicious and re-examined visually frame-by-frame. In most cases, this revealed a cell detached from the pipette or a cell heavily damaged due to destructive pulsing conditions. It should be noted here that objectivity was assured by storing all results, independent of

the quality of the experiment.

Results

Current and Voltage Clamp In general, passive electrical behaviour, like the current-voltage relationship, is determined by application of an electrical stimulus and measurement of the system response. The stimulus can be a voltage or a current while the response is the current or the voltage respectively. For linear and time invariant systems, each measurement procedure yields the same result. However, non-linear systems, like the plasma membrane of cells, show different behaviours, depending on the stimulus applied. Fig. 3 shows the response of a CHO – plasma membrane to a current stimulus. The membrane is electrically stable up to a voltage of about 200 mV. A current of ± 50 nA does not cause it to exceed this limit and is, thereby, not dramatically changing the dielectric behavior of the membrane. While some voltage-gated channels exist, even within the non excitable CHO-plasma membrane, they do not dominate the electrical response of the membrane. The membrane is charged during the first 200 to 300 µs, limited by the conductance of the membrane. Increasing the charging current will increase the voltage. When a critical voltage is reached (i.e. 0.72 V for depolarization and 0.93 V for hyperpolarization in Fig.3), membrane electroporation (MEP) occurs. Since this lowers the membrane resistance, the trans-membrane voltage drops due to the constant current.

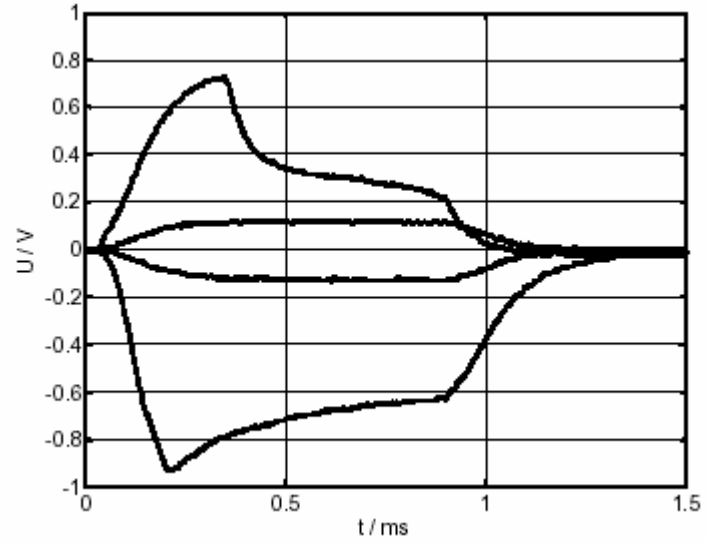

Figure 3: Transmembrane voltage due to a 1 ms current (from top: 250 nA, 50 nA, - 50 nA, -250 nA)

If the voltage across the membrane is held constant after the membrane is charged, the current continues to rise (Fig.4.). The marked difference between current and voltage clamp is the feedback. While MEP during current clamp decreases the electric field within the membrane dramatically and thereby reduces the probability of additional pore creation, the field is unchanged during voltage clamp. With respect to possible changes on the membrane, current clamp exhibits a negative feedback. While the membrane field does not change during voltage clamp, Joule heating can increase the probability of electroporation, providing positive feedback. The current increase during a constant voltage stimulus reflects the permeability increase of the membrane which, for a trans-membrane voltage below 1 V, is assumed to be due to the creation of aqueous pores spanning the lipid portion of the membrane.

Hyper- and depolarization. The CVC of membranes is measured using ramp functions, either voltage- or current-controlled. A positive stimulus first depolarizes the membrane and later re-polarizes it with the opposite polarity. A remarkable difference is the faster increase of the membrane conductance at the depolarization side (Fig.5).

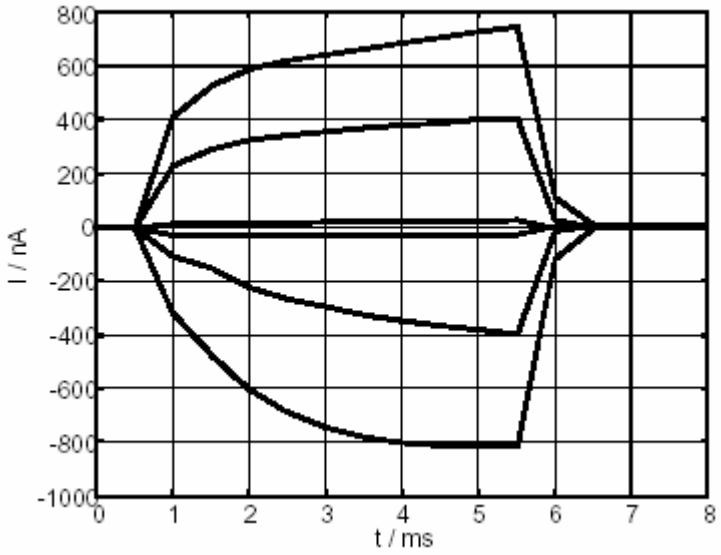

Figure 4: Transmembrane current due to the application of a constant voltage across the cell membrane. While a voltage jump across the capacitive membrane is not possible, the charging time under voltage clamp condition is on the order of 10 µs, much less than the time-scale shown for current increase in the figure. (from top: 800, 600, 200, -200, -600 – 800 mV).

Especially during current clamp experiments, we usually found a voltage regulator effect in

the cell membrane, which kept the transmembrane voltage typically in a region between 300 and 600 mV. Under both, voltage- and current-clamp conditions, a lower increase in conductance occurs during hyper-polarization. This allows the cell to reach a higher transmembrane voltage without membrane rupture. A striking result is the decline in conductance associated with the current-controlled hyperpolarization.

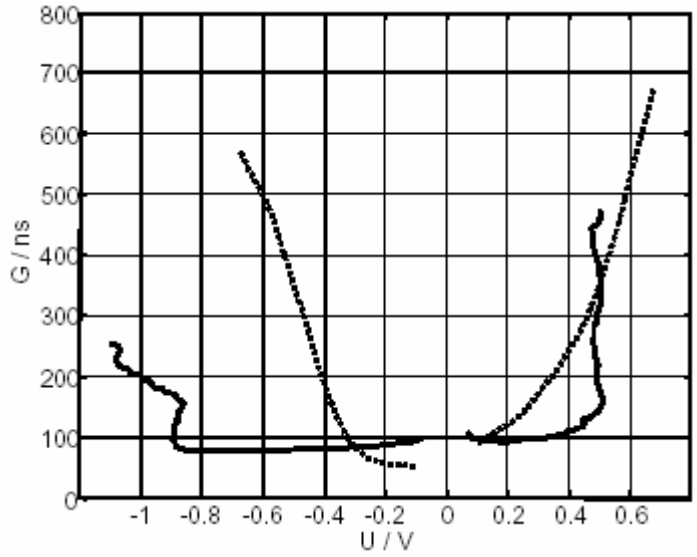

Figure 5: Membrane conductance depending on the trans-membrane voltage for comparable current and voltage clamp condition. Solid line: current clamped ramp (± 300 nA, 10 ms), dashed line: voltage clamped ramp (± 700 mV, 10 ms). The selected data show typical behavior and are chosen from a large number of experiments (about 60 interpretable experiments for these settings).

A more general view, using the averaged results for quite different conditions, as would be found in tissue or inhomogeneous cell suspensions (i.e. high concentration), is given in Fig. 6. Because the individual levels for voltage regulation are different, the clear voltage regulation appearing in current-controlled experiments is absent. Moreover, the difference for depolarization in current- and voltage-clamp conditions declines. In contrast, at hyperpolarization, almost no change in conductance was found up to 600 mV. But individual experiments, especially with slow rising ramps, already show a conductance change at much lower voltage.

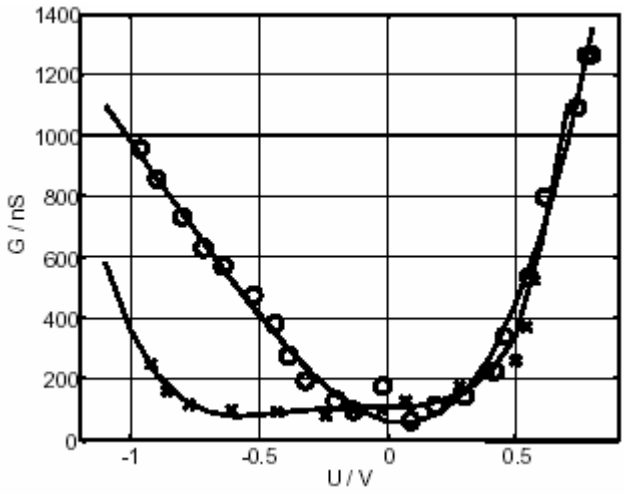

Figure 6: Membrane conductance during hyper- and depolarization averaged over all experiments (≈ 300) fulfilling the requirements for interpretation: (1) healthy looking cell, (2) cell was attached, (3) impedance before electrical stimulus was higher than 50 Ωcm^2 (4) every piece of equipment was working. The data averaged here are obtained by different persons and include different ramp rise time (5 ms .. 1s), voltage (200 mV .. 2 V, open circles) and current (50 .. 350 nA, crosses). For long-lasting stimulus, only small amplitudes are possible. Maintaining a voltage of more than 1 V is usually not possible, since the current rises to values which exceed the capabilities of the equipment (1 µA). Although a small change in the equipment would solve this limitation, the cell usually falls apart (vesicle formation) under these conditions. The values between -30 mV and 30 mV are interpolated, since the calculation of the conductance with almost zero current and alternating polarity (noise) becomes questionable.

Current/voltage characteristics depending on the slew rate. Since structural changes on the membrane level take time (Fig.3 and 4), a slowly rising ramp has a stronger effect at the same transmembrane voltage. As seen in Fig.7, with a lower slew rate, a higher conductance was achieved at lower voltage. While nothing unexpected was found during depolarization, saturation was found for hyper-polarization. In general, higher voltages without destruction of the cell was achieved during hyperpolarization.

Long lasting stimuli. If a membrane is considered to be homogeneous, composed of the same lipids at the cytosolic and the extra-cellular side, one would not expect different behavior of the membrane during de- or hyperpolarization.

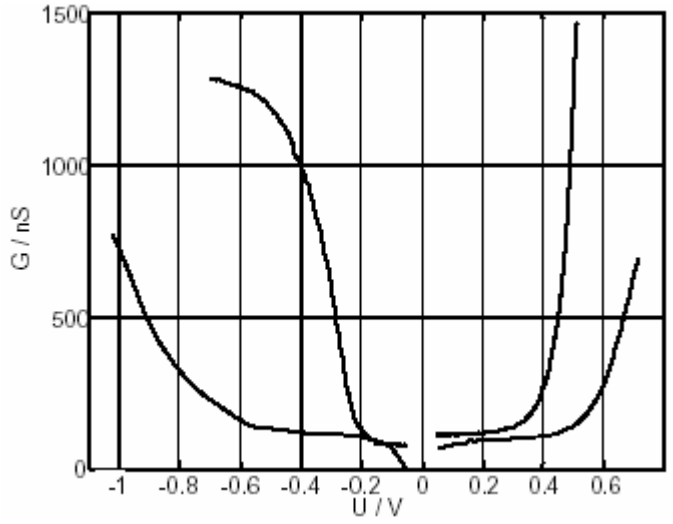

Figure 7: Current/voltage relationship for voltage clamp with different slew rate of the stimulus. From left: (-100 -5 2.5 28) V/s.

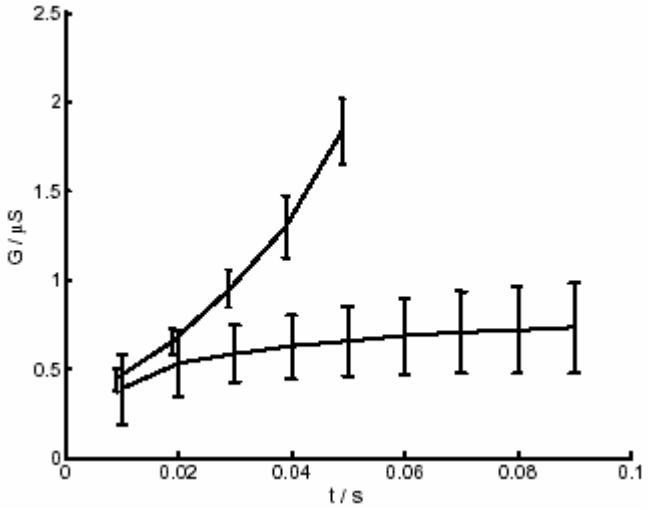

Figure 8: Membrane conductance during long lasting voltage across the plasma membrane. Upper curve U = 500 mV, N = 7, (depolarization), lower curve U = - 500 mV, N = 22 (hyper-polarization). The error bars show the standard deviation.

However, if a moderate voltage is clamped across the membrane (500 mV in Fig.8), an electrically stable membrane appears during hyperpolarization, while the conductivity in a depolarized membrane increases, resulting in complete destruction of the cell.

Discrete jumps in conductivity. With sufficiently high trans-membrane voltages (> 0.8V) dramatic structural changes on the membrane can occur instantaneously (µs-range). As shown in Fig.9, such a step can reach several hundred nS. If this is interpreted as the appearance of a huge single pore, it exceeds a diameter of 10 nm. These discrete steps

are very frequent at hyperpolarization and during voltage-clamp. They appear, however, also under current-clamp and even during depolarization. Moreover, vesicle formation (blebbing) at the cell membrane occurs very frequently during hyperpolarization but only for a destructive condition during depolarization.

Discussion

The CVC depends on the polarity of the stimulus and also on the temporal development of the stimulus. Since we investigated the membranes of living cells, voltage gated channels and active responses of the cell may influence our results. Given the voltage range below 100 mV, where active responses of the cell matter, one would already expect dramatic changes in the membrane behavior in this range. According to Fig. 3 and Fig. 4, even a stimulus of 200 mV does not dramatically change the electrical behavior of the membrane. From the current-voltage behavior below the critical level for electroporation, the passive electrical properties of the membrane (conductance, capacitance) have been estimated. The area-related conductivity of the cell membrane increases by a factor of 2 to 5 (30 – 50 mS/cm^2) compared to the prestimulus values (5 - 20 mS/cm^2). In addition, the membrane capacitance reaches 6 µF/cm^2, which is six times more than the capacitance in resting condition. The conductance and capacitance increase is mostly reversible and assumed to be due to the modulation of the Guy-Chapman – layer in the electric field.

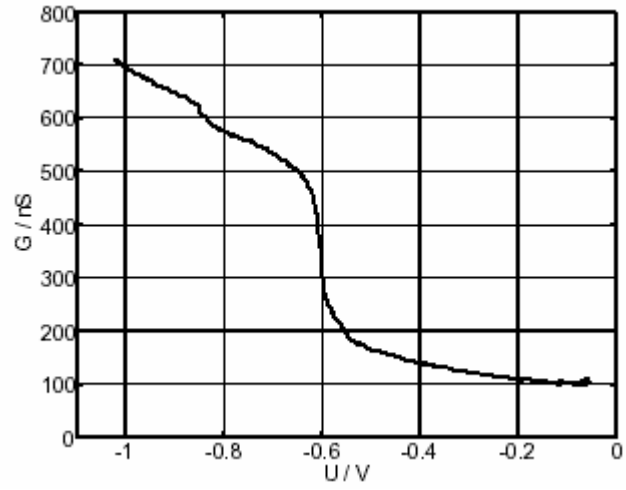

Figure 9: Step increase of the conductivity during hyper-polarization.

Once electroporation occurs, the conductivity of the membrane increases dramatically. Although it has no effect under voltage clamp conditions, the electric field within the membrane decays during current clamp. This means that current clamping exhibits a negative feedback between the stimulus and the driving force for structural changes and trans-membrane transport. This has practical relevance for electroporation of cells in low conductive media. As soon as the membrane is electroporated, the voltage divider between the membrane and the surrounding electrolytes causes a decay of the electric field. Although there is no direct positive feedback during voltage clamp, the longer the electric field lasts above the critical level, the greater the probability of further pore creation [3]. Moreover, the increased current at the same transmembrane voltage causes Joule heating which, in turn, reduces the critical voltage for electroporation, forcing further pore creation. This may be important for cell suspensions in highly conductive media. However, since the medium shunts the cell, electroporation will not dominate the electrical behavior of the suspension. This does not apply if the medium is heated only by long-lasting strong pulses. If the cells are densely packed with a highly conductive extra-cellular medium, as is found in muscles or especially within the myocardium, Joule heating due to electroporation can be important. Even with electroporation, the membrane conductivity is small compared to that of the extra-cellular medium, yielding only negligible decay in transmembrane voltage. This has even greater practical relevance since therapeutic application of electroporation involves low field (200 V/cm), long lasting pulses (10 – 200 ms) in highly conductive tissue. This does not hold for a very high electric field (> 10 kV/cm), since, under these circumstances the cell membrane shows a conductivity greater than one would expect, by replacing all lipids with electrolytes.

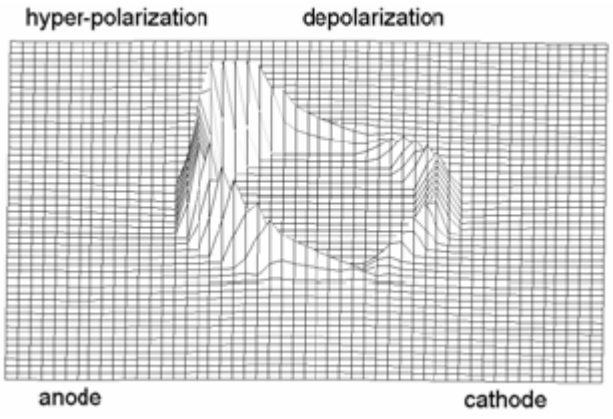

Figure 10: Simulation of the field strength for a cell in a homogenous field.

Hyperpolarization occurs at the anode side while depolarization is found at the cathode side.

It is observed in numerous studies, that most of the effects of the electric field occur at the anode side of the cell, which is the side undergoing hyperpolarization. However, the conductance increase due to electroporation is much more pronounced at the opposite side. This, however, is measured in whole cell clamp arrangement. Using the experimental CVC, it is possible to obtain approximate values of the transmembrane voltage using a finite element simulation. Fig. 10 shows features of the simulation model.

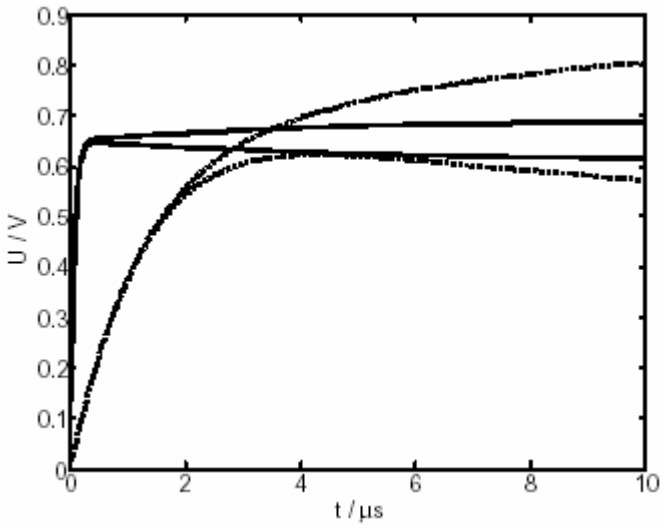

Figure 11: Estimation of the trans-membrane voltage in an electric field of 750 V/cm for a cell with 8 µm radius. Solid lines: high medium conductivity (1S/cm), dashed line low medium conductivity (10 mS/cm). The conductivity of the cytosol was set to 1.4 S/cm and the membrane capacitance was constant at 1 µF/cm2. The experimental data shown in Fig. 6 were used to calculate the voltage dependent membrane conductivity. No time varying events were simulated.

A circular-shaped cell is placed in a homogeneous electric field. At t=0 s, an electric field is turned on and the increase of the transmembrane voltage is calculated in time steps of 10-9 s, up to 10 µs. Two runs were done, one with a high and one with a low conductive medium surrounding the cell. All parameters were held constant with the exception of the membrane conductance. For the highly conductive medium, the data for the voltage clamp were used, while the current clamp data were used for the run with the low

conductive medium (Fig.11). These results show several important features: (1) the voltage at the hyperpolarization side is higher than at the opposite one, (2) the difference is less for a highly conductive medium, and (3) the charging during the first nanoseconds depends on the capacitance, rather than the conductance, of the membrane. This, however, is beyond the scope of this study. The longer charging time for the low conductivity medium is not discussed here, since this is common knowledge.

Our hypothesis is that the permeability for small ions is not important for structural changes at the membrane. The only important parameter is the electric field within the membrane and the time where critical field strength was exceeded. As estimated from the single cell experiments, but also from the simulation, the field strength at the hyperpolarization side is higher than that at the depolarization side. This increases the probability for structural changes. Due to the voltage divider between membranes and the surrounding medium, for achieving an electroporation condition, a lower applied field is necessary for high conductive media. This is consistent with the observation that tissues and pellets are easier to electroporate, even if the factor of 1.5 for the membrane field at the pole caps of single cells in suspension is taken into account. As shown in fig. 8, a long lasting stimulus below the critical field strength for immediate structural changes causes an increase in membrane permeability as well. However, this occurs more at the depolarization side. If an entire cell is considered, the conductance increase at one side will increase the transmembrane voltage at the opposite one, due to the voltage divider. Consequently, the depolarization side protects itself by lowering the membrane field. The potentially higher current is not important, since both the hyperpolarization and the depolarization side are electrically in series. But why should the hyperpolarization side show a larger permeability? As shown in fig. 9, frequent discrete steps in conductance increase occur at the hyperpolarization side. These steps are probably due to the creation of large pores, limited by the spectrin network of the cell cortex. This seems contradictory to the curved membrane of a cell; however, given the mechanical behavior of the cell cortex, the membrane between the integrenes does not show the forces in a curved membrane but behaves rather like a planar membrane. Another hypothesis is that the membrane within the electric field becomes unstable and undergoes micelle formation, since the repulsive interaction between water and the tail groups is lowered by the electric field. This becomes even more likely when the membrane is charged at a very high slew rate, so that even the self-protecting lowering of the membrane conductance does not

prevent a very high field within the membrane. Under these circumstances, an even greater effect exists, forcing water into the membrane between the head-groups and thereby making micelles a favoured structure of the lipids. As evident from impedance measurements, a recovery of the membrane takes place, suggesting that even large leaks do not necessarily cause the death of the cell.

Conclusion

It is not the dramatic conductance increase that forces large scale structural changes on the membrane level, but rather, the elevated electric field for a critical time. The depolarizing side in cell electroporation protects itself from dramatic structural changes by increasing its permeability to small ions, thereby weakening the electric field. This effect is absent at the hyperpolarization side, causing dramatic changes after a high electric field persists for a critical time. These changes may involve a mechanical rupture of the membrane or micelle formation, solubilizing the membrane. Since the electric field, not the current flow, is responsible for structural changes, one should use high electrical stimuli with a high slew rate, but short pulse duration, for cell manipulation.

Acknowledgments

This work was supported by the DFG (to EN), the European Union (to EN) and by AFOSR through a MURI grant: Sub-cellular responses to narrowband and wideband radiofrequency radiation, administered by Old Dominion University. We thank R. Nuccitelli for helpful discussion.

References

[1] HIBINO M., ITOH H., and KINOSITA K., (1992):
Time courses of cell electroporation as revealed by submicrosecond imaging of transmembrane potential, Biophys. J., 64, pp. 1789-1800.

[2] FRANTESCU C.G., PLIQUETT U., and NEUMANN E., (2002):
Electroporation of single CHO cells. in: Beckmann,D., Meister,M. (Eds.), Technische

Systeme für Biotechnologie und Umwelt, Institut fur Bioprozess- und Analysenmesstechnik, Heilbad Heiligenstadt, pp. 543-549.

[3] NEUMANN E., SOWERS A., and JORDAN C., (1989):
Electroporation and Electrofusion in Cell Biology, Plenum Press, New York

Acknowledgements

So, after 5 years, from January 2002 to August 2007, I have finally reached this point: writing the acknowledgements for my Ph.D. work.

I want to start with Prof. Dr. Eberhard Neumann, my supervisor, whom I want to thank for the opportunity to step in this field, something quite different than what I had been used to and for countless discussions about theoretical insides of electroporation. Continuing with professors, my next acknowledgement goes to Prof. Dr. Joachim Heberle for the financial support I received this last year.

In addition I want to thank my friends from this University and from outside. Together we had very good parties but also many scientific discussions.

Above and beyond that, I would also like to thank Dr. Uwe Pliquett for opening my eyes and for all the help and support he gave me. Instead of giving me the fish, he taught me how to fish.

Last but not least, I am most thankful to my wife, who gave me the moral strength to finish this work.